Revision 1

Limited channelized fluid infiltration in the Torres del Paine contact aureole

Guillaume Siron[1,2], Robert Bodner[1], Lukas Baumgartner[1], Benita Putlitz[1], Torsten Vennemann[3]

[1] *University of Lausanne, Institute of Earth Sciences, CH1015 Lausanne, Switzerland*

[2] *WiscSIMS, Department of Geosciences, University of Wisconsin-Madison, Madison, WI53706, USA*

[3] *University of Lausanne, Institute of Earth Surface Dynamics, CH1015 Lausanne, Switzerland*

Current email address: siron@wisc.edu

ABSTRACT

The metamorphic rocks from the Torres del Paine contact aureole (Patagonia, Chile) show field, petrographic, and geochemical evidences for small amounts of igneous fluid infiltration due to the solidification of the granite complex. Hydrogen isotope ratios (D/H) in the contact aureole first decrease while approaching the intrusion and subsequently increase toward the granite contact. Initial decrease with metamorphic grade is due to preferential loss of the ^{2}H isotopes due to Rayleigh fractionation during prograde dehydration reactions. The infiltration of high δD fluids from the intrusion increases δD within the last 150 m. In contrast, (^{18}O/^{16}O) ratios show no systematic changes, indicating that neither oxygen loss by Rayleigh fractionation, nor oxygen exchange by fluid infiltration was significant enough to dominate original variations seen in the oxygen isotope ratio of the protolith. Calculated volume of fluid using the position of the hydrogen isotope exchange front gives a relatively low time integrated fluid flux of about 4m^3/m^2 at the contact for the igneous fluid. These small amounts of fluid flux are in agreement with whole rock oxygen isotope data that are not affected in the contact aureole. Chlorine content of metamorphic biotite crystals, in contrast to oxygen isotopes, supports infiltration of igneous fluids. Indeed, relatively high Cl concentrations in biotite were measured in some samples close to the intrusion (up to 0.2 wt%), while chlorine concentrations in biotite are constant everywhere else in the entire contact aureole, having low concentrations (0.01-0.06 wt%). The absence of a well-marked Rayleigh fractionation trend in Cl concentrations with increasing metamorphism is surprising, since chlorine strongly fractionates into the fluid. This is best explained by slow diffusive exchange of chlorine in biotite in the cooler outer aureole. Hence recrystallization of biotite would be required to modify its Cl composition. Biotite grains from samples close to the intrusion with high Cl content also have lower Ti content (0.4 p.f.u.) than biotite (0.5 p.f.u.) from other samples containing biotite with lower Cl content located at the same distance from the contact. Since Ti content in biotite is a function of temperature, this is a good indication that magmatic fluid infiltration started post peak, early during cooling of the metamorphic rocks. Episodes of fluid-flow seemed to be nearly continuous during cooling as evidenced by numerous retrogression textures such as secondary muscovite (above 470 °C) or chlorite + muscovite intergrowth after cordierite or biotite (slightly below 470 °C). This might be related to crystallization of subsequent batches of granites, or the onset of minor fluid convection during cooling of the aureole. Nevertheless, only minor secondary muscovite has been found and fresh cordierite is present throughout the aureole confirming small amounts of fluid infiltration.

The time integrated fluid flux computed from the hydrogen isotope exchange front is two orders of magnitude lower than values computed for metacarbonate in many other contact aureoles, suggesting low permeability of pelitic rocks. In conclusion, Cl content and hydrogen isotope composition of hydrous minerals provide a sensitive tool to identify small

fluid-rock interaction events, much more sensitive than oxygen isotope compositions of the whole rock or minerals.

INTRODUCTION

Fluid-rock interaction is one the most important process on Earth. It plays an important role in mass and heat transport during metamorphism (Ferry 1986, Baumgartner and Rumble 1988, Baumgartner and Valley 2001, Cui et al. 2001, Gerdes et al. 1998), influences the stable mineral assemblages (Ferry 1986, Baumgartner and Ferry 1991, Cartwright and Buick 1996, Ferry 2000) and can drive partial melting at temperatures close to the granite solidus for metapelitic rocks (Goranson 1983, Tuttle and Bowen 1958, Luth et al. 1964, Holness and Clemens 1999) or even lower temperatures in metacarbonates as demonstrated by recently for example by Floess and Baumgartner, 2015.

Stable isotopes are one of the most common tool used to track fluid-rock interaction, especially through the measurement of oxygen isotope compositions in metacarbonates and marls (Labotka et al. 1988, Cook et al. 1997, Baumgartner et al. 1989, Holness 1997, Roselle et al. 1999), but they have been rarely used in metapelites. This is partly due to the smaller differences in terms of oxygen isotopic compositions between metapelites and typical igneous fluids. Oxygen isotopes require large amounts of fluids to register and change the large amount of oxygen contained in minerals, while hydrogen isotope compositions can trace small amounts of water infiltration, as rocks contain much smaller amounts of hydrogen (e.g., Baumgartner and Valley, 2001). The position of stable isotopes fronts has also been used to compute the amount of fluid that infiltrated a rock using transport theory (Baumgartner and Rumble 1988, Baumgartner and Valley 2001, Bickle and Naker 1990, Bowman et al. 1994, Nabelek and Labotka 1993).

A more recent tracer for fluid-rock interaction is Cl content in hydrous phases. To this date, it is mostly used in magmatic/hydrothermal systems and has not been extensively used in metamorphic petrology. The chlorine concentration in these minerals is directly linked to the HCl° activity of the fluid and the Cl solubility in silicate melts (Zhu and Sverjensky 1991, 1992, Icenhower and London 1997, Webster et al. 2015). For example, chlorine concentrations have been used to track fluid infiltration in high grade terrains using biotite Cl-contents (Higashino et al. 2013). During crystallization of magmas, chlorine becomes progressively enriched in the melt due to its incompatibility in most minerals (Speer 1984; Candela 1986, 1997). Thus, a fluid expelled during the very late stage evolution is generally enriched in chlorine. Interpreting its concentration in biotite, a major igneous or metamorphic mineral, is further controlled by crystallographic constraints, either due to Fe-Mg octahedral composition, i.e. known as the Mg-Cl avoidance rule (Munoz 1984), or the tetrahedral Al composition (Henry and Daigle 2018). Finally, Cl content in biotite seems to be very refractive and slow to exchange between biotite and fluid at medium temperatures, as highlighted recently (Siron et al. 2018a).

Here we use the Torres del Paine contact aureole (Patagonia) to compare the usefulness and sensitivity of these three different proxies to study fluid-rock interactions in metapelitic dominated contact aureoles. The Torres del Paine intrusive complex is one of the best natural laboratories to study fluid flow due to its 3D outcrop exposures (Baumgartner et al. 2007), precise geochronology and geochemical constraints on its magmatic history (Michel et al. 2008, Leuthold et al. 2012, Leuthold et al. 2013).

GEOLOGICAL SETTING

The Torres del Paine intrusive complex (TPIC) is located in the southernmost Andes in Patagonia (Chile). It consists of three major granite laccoliths, a mafic stock and a composite mafic laccolith. They intruded the Cretaceous turbidites between 12.60 and 12.43 Ma (Michel et al. 2008; Leuthold et al. 2012). The intrusion is elongated in West-East direction with a total length of about 12 km and a North-South extension of roughly 8 km (Fig. 1a). The major feeder zone of the TPIC is situated at the western end of the laccolith (Michel et al., 2008; Leuthold et al. 2013). A small, well defined contact aureole was formed in the Cretaceous Punta Barrosa and Cerro Toro Formations. These formations are mainly composed of pelites, psammites and sandstone, with minor thick (>10 m) conglomerate layers in the Cerro Toro formation (Wilson 1991; Hubbard and Schultz 2008; Fildani 2005). They also contain some minor carbonate layers with a thickness of a few centimeters to a few decimeters. This Cretaceous sequence is a thick sequence of turbidites, shed from the west into the foreland trench of the Andes (Fildani et al. 2007; Hubbard et al. 2008). The intrusion was emplaced at ca. 750 bars (Putlitz et al. 2001); pressure estimates are based on the stability of prehnite in metacarbonates, the presence of fayalite in miarolitc cavities for temperature information, as well as fluid inclusion data. For this work, a total of 5 profiles were sampled in the host rocks around the intrusion to reflect the different parts of the intrusion exposed. All samples were collected within the dark grey to black, oxide and graphite rich metapelites of the Cerro Toro Formation. Two profiles were collected above the intrusion, two at the side and one below. The different profiles are located on the map in Figure 1a (black stars). The profiles in the roof of the pluton were collected at the Cuerno Principal (CPa, Fig. 1b) and another at the Cerro Fortaleza (F, Fig. 1c). The profile on Monte Almirante Nieto comes from the side of the intrusion (A, Fig. 1d). Three more samples from the Monte Almirante Nieto (Fig. 1d) were taken on a ridge which is located about 500 m to the East than the rest of this profile (dotted line in Fig. 1d, A* in table A-1). They are treated together with the rest of the Mte. Almirante Nieto profile. The other profile located at the side of the intrusion is from the Eastern ridge of the Co. Paine Principal, in Valle Frances (VF, Fig. 1e). A profile below the intrusion is from the Cuerno Principal (CPb, Fig. 1b).

METHODS

Laser fluorination

The oxygen isotope composition of bulk rocks was determined using a CO_2 laser-fluorination technique at the stable isotope laboratory of the University of Lausanne, using a method adapted after Lacroix and Vennemann (2015). Oxygen isotope ratios are given in the standard δ-notation, expressed relative to VSMOW in permil (‰). Several aliquots of the in-house quartz standard (LS-1) were measured during each analytical session. Reproducibility for the analyses of the LS1 quartz is typically better than 0.1‰ (1SD) for two or three standards analyzed with each sequence of 12 samples.

Thermal conversion elemental analyzer (TC/EA)

Hydrogen isotope compositions were analyzed using a Thermal Conversion Elemental Analyzer (TC/EA), coupled to a Finnigan Thermo Delta Plus XL; for details on the procedure used in Lausanne see Bauer and Vennemann (2014). In-house standards (kaolinite K17 and biotite G1) were analyzed repeatedly during the sessions for normalization. Reproducibility for δD analyses of the standards is typically better than 2‰ (1SD).

Electron Microprobe Analysis (EMPA)

Major and minor element analyses of minerals were obtained with a JEOL 8200 Superprobe equipped with 5 wavelength dispersive spectrometers. The concentration of the elements Si, Al, Ti, Fe, Mg, Mn, K, Na, Ca, F and Cl were measured. The operating conditions were 15 kV, a beam current of 15 nA, with a spot size of 5 μm. Counting times were set for most elements to 15 seconds for background before and after peak and 30 seconds on the peak. Counting times were reduced for Na and K to 10 seconds on the background and 20 seconds on the peak. Fluor-phlogopite (F), scapolite (Cl), albite (Na), wollastonite (Ca), orthoclase (Si, K), andalusite (Al), fayalite (Fe), forsterite (Mg) and MnTi oxide (Mn, Ti) were used as reference standards. The data were reduced with the CITZAF matrix correction routine of Armstrong (1989). Structural formulae for biotite and muscovite were normalized to 44 charges or 22 equivalent oxygens, 8 oxygens for feldspars and 18 oxygens for cordierite. All iron was assumed as Fe^{2+}, no Fe^{3+} corrections were attempted. Cl detection limit for biotite grains were about 40 ppm weight.

RESULTS

Petrography

The metapelites of the Cerro Toro Formation in the far field of the intrusion are characterized by abundant clastic minerals. Minerals preserved are plagioclase, K-feldspar, quartz, biotite, and muscovite intermingled with newly formed clay minerals, chlorite, kaolinite, and pyrite crystallized during the Anchizone metamorphism (Süssenberger et al. 2017). The detrital grains originated from the erosion of the Patagonian Batholith and its metamorphic host rocks. The sediments were deposited on the shelf and deltas on the eastern side of the Andean orogeny and material was transported into the deep-sea trench by turbidites (Fildani et al. 2007; Hubbard et al. 2008). The outermost parts of the contact aureole are characterized by formation of hydrated minerals from these clastic precursors.

The first well defined reaction is the breakdown of chlorite (Chl), reacting with muscovite and quartz, to produce biotite (Bt) and cordierite (Crd). This evolution is typical for the low-pressure chlorite dehydration reaction. Cordierite is poikiloblastic and usually contains biotite and quartz inclusions. Biotite grain size is on the order of 10 µm; biotite crystals appear often in clusters and randomly distributed in the rocks. Metamorphic muscovite shows similar textural characteristics. Any remaining muscovite breaks down at higher metamorphic grade, reacting with biotite, to form K-feldspar (Kfs) and additional cordierite. Again, the disappearance of muscovite together with appearance of K-feldspar and newly formed cordierite is typical for the very low-pressure dehydration reaction of muscovite. Despite the aluminous character of these host rocks, no aluminosilicates have been found anywhere in the aureole of the TPIC. Hence, the TPIC contact aureole is typical for a very low-pressure environment corresponding to the 1a bathozone of Pattison and Tracy (1991). Here we will refer to the muscovite + cordierite + biotite zone as the cordierite zone and the K-feldspar + cordierite + biotite as the K-feldspar zone. The lower grade rocks that are still part of the contact aureole are referred to the chlorite zone since it is the primary mineral of these rocks.

The Torres del Paine contact aureole shows a decrease in grain size approaching the contact for most of the minerals involved in metamorphic reactions with the important exception of biotite (see below). Large detrital quartz grains can be found in the outer aureole (Fig. 2a), even within the cordierite zone where it is consumed by the chlorite breakdown reaction. Quartz and plagioclase have a more homogeneous grain size distribution at the thin section scale for rocks that experienced muscovite breakdown. Detrital muscovite can be found in the cordierite zone as coarse grains, coexisting with small, newly grown, metamorphic muscovite (Fig. 2b). These variations in mineral texture with increasing grade indicate a recrystallization of the rock matrix including the reactants when muscovite reacts out at higher temperature to form K-feldspar.

Rocks far from the intrusive contact have larger cordierite grains (Fig. 2a) than rocks close to the contact (Fig. 2f), which have typically a larger modal amount of cordierite. This indicates that the textures reflect mostly the original reaction textures, with minor recrystallization of the product mineral cordierite.

In contrast, biotite grain size has an opposite trend, exhibiting coarsening with increasing metamorphic grade. In the cordierite zone, biotite crystals are very small, e.g. less than 10 μm, often in clusters (Fig. 2b and 2c). In the K-feldspar zone, biotite grains are bigger (10-25 μm) and distributed in the rock much more homogeneously (Fig. 2d and 2e).

The Torres del Paine contact aureole rocks also show different stages of retrogression. Newly grown muscovite after K-feldspar is present in several samples (Fig. 2e), they are distinct from prograde metamorphic muscovite since they are larger in grain size. Even if cordierite is usually well preserved in the Torres del Paine contact aureole, many samples show evidence of destabilization of cordierite, e.g. it locally altered at the grain boundary (Fig. 2d), but more commonly cordierite is completely replaced by muscovite and chlorite intergrowth. Biotite can also be replaced by muscovite and chlorite (Fig 2f).

Chemical compositions of metamorphic minerals

To discuss the evolution of the compositions of metamorphic minerals in the Torres del Paine contact aureole, we will focus on the metamorphic gradient in a profile below Cuerno Principal peak. It is located underneath the intrusion. The profile is referred to as CPb. It is the most complete profile sampled, mineral assemblages can be found in supplementary material. Nevertheless, the evolution of mineral compositions is very similar for all profiles.

Muscovite. White micas in the CPb profile are very close to the muscovite end-member compositions with a small amount of phengite component (i.e. FeO content ranging from 0.99 to 2.03 wt% and MgO content between 0.52 and 1.46 wt%; see Table 1). This corresponds to a low phengite component (calculated using $^{VI}R^{2+}/(^{VI}R^{2+} + {}^{VI}R^{3+})$) from 0.052 to 0.126. The two lowest grade samples (07TP55 and 07TP56), located at a distance of respectively 400 m and 300 m from the contact with the intrusion have the highest $^{VI}R^{2+}$ content. There is no correlation between paragonite content and distance from the intrusion. F and Cl contents are very low, with 0.04-0.08 wt% (0.018-0.030 p.f.u.) for F content and mostly below detection limit for Cl content, i.e. ≈ 0.004 wt% (below 0.001 p.f.u.). At these levels, no trend was observed in the contact aureole with the precision of EMPA.

Feldspars. Plagioclase is present in all samples from the CPb profile, usually with two distinct compositions due to the peristerite gap at these temperatures (470-600 °C, see Table 2). Metamorphic albite is in equilibrium with an oligoclase of decreasing X_{An} (calculated as Na / (Na + Ca + K)) with increasing peak temperature, with $X_{An} = 0.270$ at 300 m and $X_{An} = 0.166$ at 150 m, respectively. Close to the contact with the intrusion there is only one plagioclase composition, with $X_{An} = 0.217$. In contrast, Sample 07TP63 (at 10 m) has two very distinct populations of plagioclase of $X_{An} = 0.359$ and $X_{An} = 0.786$. These are completely different from the rest of the profile. This sample also exhibits clinozoisite-rich epidotes, calcite grains showing the influence of the second part of the thin section, which is a meta-carbonate.

K-feldspar is present as sedimentary relicts at lower metamorphic grades up and into the cordierite zone as well as a product of the muscovite dehydration reaction in the K-feldspar zone. The X_{Ab} (Na / (Na + Ca + K)) component is comprised between 0.154 and 0.222 (Table 2). The compositions of these two different generations are not different.

Biotite. Biotite compositions have high octahedral Al (^{VI}Al), as often in low pressure metamorphic rocks (see Table 3). The X_{Mg} and Ti contents have two opposite trends with increasing temperature for most samples. The X_{Mg} decreases toward the contact with the intrusion and Ti content increases. The X_{Mg} range from 0.389 at 400 m to 0.355 at 5 m and the Ti content (based on 44 charges or 22 equivalent oxygens formulae) from 0.161 p.f.u. at 400 m to 0.463 p.f.u. at 5 m (Fig. 3a). Both X_{Mg} and Ti contents show a large range along this trend, especially visible for sample 07TP58 (grey squares, Fig. 3a). Two samples fall clearly off this trend, i.e. 07TP63 (at 10 m) and 10TP57 (at 1 m). Interestingly, the only difference between these two samples and the rest of the samples is their Cl content (Fig. 3b), they both have higher Cl concentrations, i.e. 0.16-0.18 wt% (0.041-0.046 p.f.u.) versus 0.01-0.02 wt% (0.002-0.004 p.f.u.) for the other samples. F content was difficult to determine because of the Fe interference when using a large crystal (LDE1) for the determination of fluorine concentrations with EPMA. F contents in amphibolite facies biotite grains from contact aureoles are usually about 0.2-0.4 wt% (Sisson 1987, Siron et al. 2018a).

Cordierite. As for the biotite of the CPb gradient, cordierite shows a decrease in X_{Mg} toward the contact with the intrusion, from 0.539 to 0.505, except close to the intrusion where sample 10TP54 has a slightly higher XMg of 0.52 (see Table 4). Cordierite does not contain measurable amounts of Cl, either below or slightly above the detection limit (0.004 wt%).

Thermodynamic modelling

Pseudosections were computed using version 6.6.6 of the Perple_X software (Connolly 2009). Due to the small variations in bulk rock composition of the Torres del Paine samples (see Fig. 4), sample 07TP56 was chosen for pseudosection calculations, since its composition is typical for the metapelites of the TPIC contact aureole. The composition used for thermodynamic modelling comes from XRF analyses, oxide composition can be found in the supplementary materials. Ti has been excluded from the composition by projection through ilmenite (i.e. associated Fe moles were subtracted from the bulk rock composition), no correction for Ti in biotite was attempted since it is usually low (below 0.5 p.f.u.). Since graphite is present in most samples, C was set as a saturated component and fluid compositions were calculated using the equation of state (EoS) by Connolly and Cesare

(1993, EoS 10 in Perple_X). An X_O of 1/3 was set to impose a saturated H_2O rich fluid (see Connolly and Cesare (1993) for a discussion of this variable). This choice was made since the fluid produced from the successive dehydration reactions is mostly H_2O. Hence, water-rich conditions most likely prevailed during contact metamorphism of metapelites in the Torres del Paine contact aureole. The choice of a reduced water activity using this fluid EoS instead of imposing a pure H_2O fluid phase using the CORK equation of state from Holland and Powell (1991) results in a small shift of the dehydration reactions towards lower temperatures (less than 20 °C).

Even if bulk rock compositional variations are very small, this could still translate into large differences for calculated locations of the reactions, depending on the sensitivity of each individual reactions to variations of composition. The most important component in the case of metapelite is the bulk rock Fe/(Mg+Fe) ratio. Fig. 5a shows the impact of Fe/Mg variations for the composition of a typical rock from the aureole (07TP56). Interestingly, temperatures do not change much for the X_{Mg} range of 0.36-0.5, which represents the extend of bulk rock variations for the rocks of the Torres del Paine contact aureole. Both isograds, the crd-in (field 1) and kfs-in (field 3), are only slightly displaced in temperature (<10 °C) with changes in X_{Mg}. The temperature for the bt-in isograd (field 2) is not affected by changes in bulk rock composition (Fig. 5a). This agrees well with the appearance of cordierite at approximately the same distance from the intrusion in all pelitic compositions, allowing to readily map the isograd (Fig. 5a).

Pressure has been estimated based on assemblages in meta-marls to be 75MPa (Putlitz et al., 2001; Baumgartner et al., 2007). This is consistent with the absence of aluminosilicate, which also indicates very low-pressure metamorphism. Figure 5b shows a phase diagram calculated for the composition of the representative pelite sample, 07TP56. The temperatures are 470 °C for crd-in isograd and 520 °C for kfs-in isograd (Fig. 5b).

Figure 5c shows the calculated volume percent of the major phases in the rock, in good agreement with the observed mineralogical evolution in the aureole. Even if cordierite is stable at slightly lower temperature than biotite, the major episode of cordierite growth is related to the chlorite breakdown reaction with cordierite and biotite as products of this reaction (Fig. 5c). The second episode of growth for cordierite occurred during the muscovite breakdown reaction, where metamorphic K-feldspar is produced. Fe and Mg of cordierite is obtained from biotite, resulting in a minor consumption of biotite (Fig. 5c).

Field observations of fluid flow

The Torres del Paine intrusion has abundant miarolitic cavities in all granitic and most mafic intrusive rocks. Cavities are more abundant towards the borders of the intrusion and modal abundance of cavities can reach up to 20-30% in the most external parts of the oldest granite, the granite I, also called Almirante granite (Michel et al., 2007; Baumgartner et al., 2007; Leuthold et al., 2013). These rocks are fined-grained and have graphic quartz-feldspar intergrowths. The cavities are typically isolated, but they can form in some rare cases interconnected tube-like structures surrounded by granite grus. These cavities mark igneous fluid exsolution upon cooling and solidification of the granite. The cavities are filled mainly with euhedral quartz and feldspars, as well as with fayalite, tourmaline, chlorite, pyrite, zeolites and carbonates (Bégué et al. 2018). Some miaroles are completely filled with coarse quartz, forming pods up to one meter in size. These textures indicate a granite melt with near-eutectic composition, which was highly water saturated. At a pressure of 75 MPa – the likely emplacement pressure (see above) water saturation of a granitic magma is reached at ca. 3 wt% of water (Holtz et al. 1995).

Fluid infiltration textures – veins, or bleaching zone, skarns, etc. – are rarely visible in the host rocks, despite the fact that the contact is extremely well exposed (see Fig. 1). The only obvious features are small bundles of veins which continue on strike from the dyke tips emanating into the host rocks (Bégué et al. 2018). Numerous dykes emanate from the intrusion into the host rock on the Eastern end of the intrusion, as well as on the North and South side of the intrusion. These dykes are similar to ring dykes in that they emanate from the rim of the intrusion about vertically from the contact, dipping towards the center of the intrusion (Fig. 6a). Their spacing is a few hundred meters in the roof. They start from within the intrusion and can be followed for tens and up to a hundred meters into the host rock. They explode into a myriad of dyklets about halfway along their length. Each dyklet is continued by a fissure-like vein, which sometimes produces pyrite-amphibole veins surrounded by bleached zones in the metacarbonates and metapelites. The veins are maximum several millimeters wide, surrounded by a bleaching zone of a few centimeters' width (Fig. 6b). The bleaching zone is due to the oxidation of the organic matter present in the sedimentary rocks. Fluid infiltration is localized along these veins. Similar bleaching zones can be found in the metasediments close to the contact. The zone is typically less than 1 meter wide, and only visible locally.

Stable isotope compositions

Oxygen and hydrogen isotope compositions of the Torres del Paine igneous complex.

Whole rock oxygen isotope compositions range for mafic rocks from 5.5‰ to 7.8‰ for gabbronorites, gabbros, and diorites, with the diorites having the lowest δ^{18}O values (Leuthold 2011). Granite oxygen isotope ratios vary between 7.1 to 9.1‰. Oxygen isotopes range from 9.1 to 9.9‰ for quartz and 5.1 to 6.0‰ for biotite (Table 5). These values fall into the field characteristic for A-type granitic plutons (Sheppard 1986). Quartz in miarolitic cavities shows a slightly wider range in δ^{18}O values of 8.8 to 11.1‰ (Table 5), but they overlap with the quartz values of the granites. Oxygen isotope thermometry on fayalite-quartz pairs from miarolitic cavities give a temperature of 750 ± 30 °C (Putlitz et al. 2001). The pressure derived from the solidus for a haplogranitic melt at this temperature is about 750 bar (Luth 1964). This is in good agreement with available estimates based on meta-marls (Putlitz et al. 2001). Quartz-biotite pairs from the granites give 600 to 640 °C. The fact that biotite is a fast diffuser for oxygen (e.g. Eiler et al., 1993) and that solidus temperature at these pressures are much higher (≈ 730-750°C, Johannes and Holtz, 1996), indicates that these are most likely closure temperatures and not crystallization temperatures.

Hydrogen isotope values of magmatic biotite from the different granites of the Torres del Paine complex span a narrow range of -97 to -83‰ (Table 5). Indeed, only one sample has a δD value of -126‰. The biotite grains of Almirante granite (granite I, Michel et al. 2008) have values between -97 and -95‰, which are slightly lower than those for Cathedral granite (Granite III, Michel et al., 2008), with biotite values between -88 and -83‰ (Table 5) typical for granite derived biotite. The granite I values are depleted in D relative to typical δD values for granites (e.g., Sheppard 1986).

Oxygen and hydrogen isotope composition of the host rock. Bulk rock oxygen and hydrogen isotopes ratios have been determined for the profiles above and below the Cuerno Principal, as well as for the profiles at Co. Fortaleza and at the Mte. Almirante Nieto. Several samples far from the contact aureole have also been analyzed in order to evaluate the initial heterogeneity of the protolith. They are plotted schematically on the right-hand side of the diagrams of Figure 7.

Host rock oxygen isotopes. Within each profile, bulk rock oxygen isotope compositions were found to be homogeneous at the scale of about 1‰ (Table 6 and Figure 7a). However, comparison of the different profiles shows differences. Especially, the profile below the intrusion at Cuerno Principal has oxygen isotope values which are approximately 1‰ higher than in other profiles, between 13.9 and 15.1‰, compared to 12.8 to 14.1‰ for other profiles, respectively. But taking into account all profiles, the $\delta^{18}O$ values still overlap with initial heterogeneity (between 12.7 to 15.1‰), i.e. protolith values of the samples outside the aureole (dashed lines in Fig. 7a). Only three samples (two from the profile above Cuerno Principal and one from the Monte Almirante profile) have oxygen isotopes composition which is distinct from the rest. They are found at distances of 155, 215 and 250 m from the intrusion. A microscopic inspection reveals that these samples are texturally different, containing coarse clasts (>1 mm) of quartz and feldspar. The presence of larger feldspar and quartz clasts identify them as aluminium-rich, immature psammites, while the other samples had a fine-grained protolith with only small clasts (<200 μm). Hence, we suggest that the low isotopic values reflect different protolith compositions for these samples.

Two additional samples have low $\delta^{18}O$ values between 9.8 to 10.0‰. They were collected very close to the intrusion (<1 m away from the contact). They lost their organic carbon and are bleached (see fig. 6b).

Host rock hydrogen isotopes. The hydrogen isotope data show a clear pattern on the aureole scale, in contrast to the oxygen isotope compositions (Table 6 and figure 7b). This is best seen in two profiles; one below the intrusion (Cuerno Principal below) and one above the granite (Monte Almirante Nieto; Fig. 7b). In these two profiles, the δD values decrease first towards the intrusion up to about 150 m from the contact, where a value as low as -104‰ was measured in the Monte Almirante profile. Subsequently, the hydrogen isotope ratios increase again closer to the intrusion, to reach a maximum at the contact, with values of -82‰. The hydrogen is mainly carried by biotite, thus in the samples close to the intrusion it can be directly compared to values of the granites, where the main hydrogen carrier is also biotite. They are very similar to the values of the granites, in which biotites vary between -97 and -83‰ (see above).

Chlorine content in igneous and metamorphic biotites

Chlorine content in igneous biotites. The chlorine content of biotite of four samples from the granitic complex varies between 0.3 and 0.8 wt%. This corresponds to a Cl content of 0.08-0.22 p.f.u. and a molar fraction X_{Cl} = 0.02-0.05. These somewhat high chlorine concentrations are consistent with a progressive enrichment of the Magmatic Volatile Phase (MVP) due to the incompatibility of Cl with the crystallizing minerals. The biotite has a high iron content in these granites, with X_{Mg} between 0.15 and 0.32.

Chlorine content in metamorphic biotite. Figure 8 shows the chlorine content in biotite for each profile collected in the contact aureole. Chlorine concentrations are almost always very low, i.e. below 0.05 wt% (0.015 p.f.u.). Chlorine concentration is sample dependent, but it also varies within each sample. In contrast to hydrogen isotopes, no systematic variations with the distance from the intrusion are found on the large scale. Nevertheless, four samples collected just next to the intrusion have higher Cl contents in biotite than the rest of samples. Chlorine concentrations in biotite in the distal aureole varies between 0.01-0.06 wt% (Fig. 8f). while chlorine concentrations in biotite close to the contact can reach values of up to 0.18 wt% (0.05 p.f.u.). Indeed, four samples have high chlorine concentrations. They are samples from three different profiles: two samples from the profile below the granite at Cuerno Principal (Fig. 8a), one sample from the Valle Frances side profile (Fig. 8e), and one sample from the profile above the granite at Mte. Almirante Nieto (Fig. 8c). They all are from the immediate proximity of the granite, less than 20 m away from the contact. These high values are 3 to 10 times higher than those observed in distal host rocks.

Figure 9 reveals no correlation between Cl content and X_{Mg} biotite grains. This is true for biotite grains from different samples within a specific profile, as well as between profiles.

Indeed, in the Cuerno Principal below profile, the two samples with a high Cl content have both higher X_{Mg} than the samples with low Cl content. In addition, no correlation between Al^{iv} or Ti content has been found.

DISCUSSION

Both bulk rock hydrogen isotope compositions and chlorine content in biotite change close to the contact between intrusive rocks and surrounding metamorphic rocks. Characteristic are higher δD values (whole rock) and a higher Cl content in biotite in some samples. These data provide good evidence that the Torres del Paine contact aureole experienced igneous fluid infiltration. Oxygen isotope compositions do not show significant trends. In the distal aureole, hydrogen isotope compositions again show a clear trend with a marked decrease in δD values approaching the contact. In contrast, neither chlorine concentrations nor oxygen isotope ratios show any trend in the distal aureole. The following section discusses the different behavior of these three potential markers of fluid-rock interactions in terms of equilibrium vs disequilibrium processes and scale of equilibration vs time integrated fluid flux.

Significance of bulk rock δD variations

Hydrogen is present in biotite in the K-feldspar zone, and in biotite and muscovite in the cordierite zone. Hydrogen can also be stored in the channels of cordierite in both zones, but in much lesser amount compared to muscovite and biotite. At lower temperature, most of the hydrogen is bound in chlorite and muscovite. Trace amounts of apatite are present in some rocks in the Torres del Paine contact aureole; but its fraction is too small to have a significant effect on the hydrogen balance. Since kinetics of isotopic exchange by recrystallization is orders of magnitude faster than by diffusion (Baumgartner and Valley 2001; Putnis et al. 2007), hydrogen isotopes in the Torres del Paine should monitor fluid-rock interactions most efficiently, since all of the major hydrous phases are involved in dehydration reactions.

Indeed, the different hydrogen isotope profiles of the Torres del Paine do vary in the contact aureole (Fig. 7b), showing a decrease of the δD values when approaching the intrusion in the outer part of the aureole (>150 m from the intrusion) and an increase in the inner part of the aureole. We interpret these two trends as being the consequence of two very different processes of fluid-rock interaction: (i) metamorphic dehydration reactions and (ii) magmatic fluid infiltration. The two processes are described below.

The decrease of the δD value in the chlorite and cordierite zones is interpreted to reflect Rayleigh fractionation due to dehydration reactions. At these temperatures, water is enriched in deuterium with respect to hydrous silicates (Suzuoki and Epstein, 1976). Hence, water removed from the rocks takes up a disproportionately high amount of deuterium. The remaining hydrogen bound in the mineral structures contains a disproportionately low amount of deuterium.

The calculation below assumes that the removed water was in isotopic equilibrium with biotite. Assuming a temperature of 480 °C, corresponding to the temperature of the chlorite breakdown (see Fig. 3) it can be estimated that about 40% of the water contained initially in the hydrous silicates needs to be removed to produce the ca. 20‰ change in δD values (α_{bt-H_2O}= 0.95453, Suzuoki and Epstein, 1976). At a temperature of 520 °C approximately 45% of the water has to be removed. The overall amounts of removed hydrous fluids agrees with the actual water loss estimated from phase petrology calculations. Given the sharpness of the isograds, one would expect from these estimates a step-like decrease in δD. The relatively smooth decrease is expected if reaction kinetics is sluggish, so that the individual reactions occur over a temperature range of ca. 50 °C or if the initial profile is changed by small amounts of diffusion, dispersion, and fluid flow. Crystal size analysis and thermal modelling by Bodner et al. (2013) suggest that, indeed, reaction progress can span several tens of °C. Furthermore, the presence of larger, detrital grains of biotite or quartz is a good indication that large amount of textural disequilibrium exists in the Torres del Paine contact aureole. Also, in other contact aureoles, evidences for sluggish reaction kinetics are well established. Inconsistencies between isograd locations (Waters and Lovegrove 2002; Pattison and Tinkham, 2009) or thin section scale heterogeneity for Cl and F contents in biotite (Siron et al. 2018a) are common in metapelitic contact aureoles. Heterogeneity within samples for oxygen isotope compositions (Ferry et al. 2013) or calcite-dolomite thermometry (Müller et al. 2008) have been shown for metacarbonate contact aureoles. Both evidences are good indications that metamorphic reactions do not progress according to the equilibrium paradigm in contact aureoles.

Close to the contact (at about 150 m) the δD values increase and become similar to those of biotite in the granites. This is interpreted as the result of magmatic fluid infiltration. A rough estimate of fluid flux can be obtained using the distance of the δD-front (demarking the most notable change in values) from the contact with the intrusion, which is assumed to be the source of the fluids. Maximum estimates of the amount of fluid flow needed are computed, in order to determine the potential effect of fluid flow on contact metamorphism in the Torres del Paine. Additional details on these estimates can be found in Baumgartner and Rumble (1988) and Baumgartner and Valley (2001).

For the stable isotope transport theory, the isotopic exchange front lags behind the actual fluid front. The difference in front speed between fluid and tracer (here bulk rock δD) is termed the retardation factor and can be described by the relation:

$$\frac{v_f \cdot t}{v_\delta \cdot t} = \kappa \qquad (1)$$

where κ represents the retardation factor, v_f is the velocity of the fluid front, v_δ the velocity of the isotope front and t stands for time. The combination $v_i \cdot t$ represents the distance of front i (i = isotope (δ) or fluid (f)) from the intrusion. The retardation factor κ can be approximated by the equilibrium constant K_D between fluid and rock,

$$\kappa \approx K_D = \alpha \frac{\beta_s \bar{V}_f}{\beta_f \bar{V}_s} \qquad (2)$$

Here, β is the stoichiometry of hydrogen in the solid (s) and the fluid (f), α the fractionation factor from Suzuoki and Epstein (1976), and $\bar{V}$ the molar volume of the respective phases, i.e. 52 $cm^3 \cdot mol^{-1}$ for a fluid composed of pure water and 153 $cm^3 \cdot mol^{-1}$ for biotite. Equation (2) is valid for small porosities only (Baumgartner and Rumble, 1988). A contact temperature of 550 °C is used, along with a typical modal abundance of 10% by volume of biotite in the rock. This results in a K_D of 3.6. Using the largest distance of the isotope front of 150 m (Fig. 7b), a time integrated fluid flux of roughly $4m^3 / m^2$ is obtained.

This value shall be compared with values from the literature. Bowman et al. (1994) calculated about 500 m^3/m^2 based on oxygen isotope compositional changes in siliceous dolomite around the Alta stock. Similarly, Nabelek and Labotka (1993) obtained 720 m^3/m^2 to produce the oxygen isotope composition in the Notch Peak contact aureole. Hence, the value registered by the rocks in the Torres del Paine is very small, ca. 100 times less, compared to other contact aureoles. Such small amounts of fluid infiltration might be typical for metapelite dominated aureoles, where the host rocks have a relatively small permeability when compared to metacarbonate dominated aureoles.

Lack of $\delta^{18}O$ fronts in the aureole

Rayleigh fractionation effects have been shown to be very small for a major element like oxygen, since only a very small fraction of oxygen is accessible for fast isotopic equilibration during dehydration reactions of a typical metapelite. In addition, the fractionation between oxygen in the fluid phase and metamorphic minerals is relatively small compared to hydrogen (maximum several permille). As a consequence, the oxygen isotope composition typically is not changed by Rayleigh fractionation alone (Bumgartner and Valley, 2001).

The absence of an oxygen isotope infiltration front in the Torres del Paine contact aureole can be explained by two factors: 1) The fluid expelled from the intrusion has a composition similar to a fluid in equilibrium with the minerals in the metapelites. This is in contrast to metacarbonate rocks, where a difference between host rock and fluid expelled from the intrusion can be as high as 15‰. 2) Oxygen being a major element within minerals, a small amount of infiltrated fluid, even when reacting with the minerals, cannot produce a well recognizable infiltration front for $\delta^{18}O$ because of simple mass balance constrains. In addition to that, using the time integrated fluid flux determined from hydrogen isotopes, the position of the oxygen isotope infiltration front would lie within the first meter of the contact. The sampling strategy chosen for this study does not allow a spatial resolution of 1 m or less, which would be required to characterize a 1 m oxygen isotope front. The fact that some samples have very low $\delta^{18}O$ values at the contact could support infiltration of a small amount of fluid. Nevertheless, the high background-variability of $\delta^{18}O$ values for the metasedimentary rocks also does not allow well-defined oxygen isotope depletion zones to be present in the Torres del Paine contact aureole.

Cl content in biotite

The third tracer used to investigate fluid flow is the chlorine content of biotite. Figure 9 illustrates that the Cl content is not correlated with X_{Mg} and hence not constrained by variations of the crystal lattice in the aureole. It follows that the higher Cl contents close to the contact are most probably due to fluid infiltration. Cl content of hydrous minerals are linked to the HCl° activity in the fluid (Zhu and Sverjensky 1991, 1992). The HCl° activity is a function of two major variables, the pH of the fluid (Eugster and Baumgartner 1987) and the total Cl dissolved in the fluid (Zhu and Sverjensky 1991). Thus, any change in the mineral assemblage in equilibrium with the fluid will result in a change in pH and HCl° activity, and by consequence Cl content in hydrous minerals. Therefore, changes in Cl content of hydrous minerals can be either the result of the appearance or disappearance of a metamorphic mineral due to metamorphic reactions or change in the total Cl dissolved in the fluid due to the infiltration of an external fluid, dilution/desiccation of the residual fluid.

Recently, Siron et al. (2018a) have documented the slow kinetics of exchange for the O(4) site of biotite during contact metamorphism, especially for Cl. It seems that the Cl content does not change during contact metamorphism, unless biotite grains recrystallize, when they can exchange with a fluid of different chlorinity or under different pH conditions, if such a fluid is present at that moment. This may account for the absence of a trend in Cl concentrations of biotite within the cordierite zone. In contrast to hydrogen isotopes, the Cl content in biotite does not record Rayleigh fractionation, even though Cl fractionates strongly into the fluid, and hence Cl is incompatible with biotite. Thus, Cl should be strongly depleted by Rayleigh fractionation. Such discrepancy between the expected behavior and the actual measurements requires an explanation.

Disequilibrium might be an appropriate explanation. If Cl only exchanges for the part that reacts, Cl cannot be depleted in the whole crystal; hence no Rayleigh fractionation occurs. Such a disequilibrium behavior is not unexpected in the case of the Torres del Paine contact aureole, since various examples of disequilibrium can be found, i.e. presence of clastic minerals, even in the cordierite zone (Fig. 2a and 2b), as well as large variations in the X_{Mg} and Ti content of biotite (Fig. 3a).

The biotite grains that have high Cl content close to the intrusion are clearly larger, with a well-defined habitus compared to the patchy, small, biotite grains observed in the cordierite zone. This provides good evidence that the large biotite crystals recrystallized and were thus able to exchange their composition with a fluid of different HCl° activity. The fact that not all samples from the K-feldspar zone have a high Cl content in biotite is a good argument against a potential pH influence. If the high Cl contents in biotite were the result of a change in pH due to the shift from muscovite to K-feldspar for the KCl° buffer, all samples close to the contact should be affected, not only a few. Together, these arguments allow the interpretation that the high Cl content in biotite – as well as the bulk rock hydrogen isotope compositions - are the result of the infiltration of igneous fluid. Moreover, since only a few samples have these relatively high Cl contents, the infiltration seems to have been channelized and does not represent a major percolation of fluids. This interpretation is consistent with the very low time integrated fluid flux computed from hydrogen isotopes compositions in the contact aureole.

The sample 07TP63 is slightly different since it is in contact with a carbonate layer. This sample provides evidence of CO_2 infiltration, i.e. clinozoisite-rich epidotes, calcite grains, higher X_{An} composition of plagioclases. In this case the high Cl content in biotite might be due to fluid immiscibility, well known in the case of H_2O-CO_2-NaCl fluids (Aranovich 2010), instead of igneous fluid infiltration. Nevertheless, since only this sample was close to a metacarbonate layer, this does not change the overall interpretation of high Cl content in biotite resulting from igneous fluid infiltration.

Timing of fluid infiltration

Fluid infiltration can have a major effect on heat and mass transport. It is important to understand the timing of fluid infiltration because it could, for example, increase peak metamorphic temperatures if infiltration occurs close to the peak metamorphism in the contact environment, or promote short cooling times (e.g. Cook and Bowman 1994, Hanson 1995). Below is an attempt to identify the relative timing of fluid infiltration in the Torres del Paine contact aureole.

The granites of the Torres del Paine laccolith are typical A-type granites (Michel et al. 2008), which can be hot and relatively dry (King et al. 2001). These dry granites become water saturated at the very end of cooling, after a substantial degree of crystallization. This is supported by the quartz-fayalite temperatures of 750°C measured in the miaroles of the granite I. This would imply that fluid expulsion occurred at a late stage of granite crystallization.

The major element composition of metamorphic biotite shows that biotite grains with high Cl content have slightly lower Ti contents compared to biotite from samples located at the same distance (or close) to the intrusion. Since the Ti content is strongly linked to the temperature (Henry and Guidotti 2002, Henry et al. 2005), this indicates that the biotite grains with a high Cl content have recrystallized in equilibrium with the high salinity fluid from the intrusion during the onset of cooling. While post peak, fluid infiltration must have occurred above the lower stability limit of biotite, which is about 470 °C (Fig. 5). Ti-in-biotite for samples from the Torres del Paine contact aureole are very different than temperatures deciphered from mineral assemblages, sometimes even more than 100 °C (Table 3). This can be either due to disequilibrium or the fact that aluminosilicates are not present, and hence, the Torres del Paine metamorphic rocks have a different buffer assemblage than what was used to constrain this geothermometer. Nevertheless, the overall trend of decreasing temperature with distance to the contact for low Cl content samples is also observed for Ti-in-biotite temperatures.

Similarly, high Cl contents biotite grains have lower Ti-in-biotite temperatures than low Cl contents located at similar distance from the contact.

Retrograde muscovite after K-feldspar provides evidence of fluid infiltration during cooling of the surrounding rocks, at a still relatively high temperature, i.e. between the K-feldspar-in isograd (520 °C) and the biotite and cordierite isograd (470 °C). Chlorite-muscovite alteration of cordierite or biotite represent fluid infiltration at temperatures below 470 °C.

Figure 10 sketches the interpretation of the temperature-time evolution for a metapelite at the contact between the intrusion and the surrounding rocks. Overall time for cooling of the Torres del Paine intrusion can be estimated using simple 1-d thermal models (e.g. Spear, 1993). The time span shown corresponds to about 20 ky for the cooling of an 800 m intrusion. Since the three different markers of fluid infiltration, i.e. a high chlorine content, a δD infiltration front, and the retrograde muscovite and finally chlorite + muscovite intergrowth after cordierite and biotite, occur within a 15 ky window, it is very unlikely that they represent three distinct fluid infiltration events but rather the nearly continuous emplacement/crystallization of the different pulses of granites of the Torres del Paine laccolith.

IMPLICATIONS

The comparison of these three different tracers for fluid rock-interactions shows the need to carefully evaluate which one is appropriate in the environment to be studied. In the case of metapelites, low concentration tracers are easier to exchange, and hydrogen isotopes or Cl content in hydrous minerals will be more sensitive to fluid-rock interactions than oxygen isotope compositions. This might open the possibility to reassess the extend of fluid flow in metapelite dominated aureoles, where clear evidences of igneous fluid flow has so far not been commonly observed. Using chlorine in hydrous minerals provides an exciting avenue for studying fluid-rock interaction in this kind of environment. Nevertheless, the fact that Cl content in hydrous minerals, such as biotite, exchange very slowly at low to medium temperatures requires carefull petrologic studies to identify newly crystallizing phases or re-crystallization of pre-existing phases.

Additionally, the observation of a Rayleigh fractionation trend for hydrogen isotope during chlorite breakdown reaction show the potential of this tracer to study fluid-rock interactions during internal fluid production where the fluid isotopic composition is in equilibrium with the rock composition. Fluid-rock interactions during dehydration reactions is a key component to understand porosity creation and is necessary to obtain connected pores (Plumper et al. 2017) and slip events created due to fluid overpressure (Taetz et al. 2018). To date, only a few studies have focused on hydrogen isotopes from metamorphic minerals during prograde metamorphism. However, all of these studies used mineral separates and never analyzed the hydrogen isotope composition of metamorphic minerals within the context of their textural positions. The recent development of new SIMS reference materials (Siron et al. 2018b, Luisier et al. 2019) will promote the use of hydrogen isotopes and water content since these can know be measured in-situ in micas.

ACKNOLEDGEMENTS

We thank Darrell Henry and Simon Harley for extensive comments on an earlier version of the manuscript. Funding was provided for this project to L.P. Baumgartner by SNF grants 200021_153094 and 200020_140974 and the KIP 6, PCI CASA, grant are gratefully acknowledged.

REFERENCES

Armstrong J.T. (1989) CITZAF: Combined ZAF and Phi-Rho (Z) Electron Beam Correction Program, California Institute of Technology, Pasadena, CA.

Bauer, K.K., and Vennemann, T.W. (2014) Analytical methods for the measurement of hydrogen isotope composition and water content in clay minerals by TC/EA. Chemical Geology, 363, 229–240.

Baumgartner, L. P. and Rumble, D. (1988) Transport of stable isotopes: I: Development of a kinetic continuum theory for stable isotope transport. Contributions to Mineralogy and Petrology, 98, 417–430.

Baumgartner, L. P., Gieré, R., Trommsdorff, V., and Ulmer, P. (1989) Field guide for the Southern Adamello. in Guidebook for the excursion to the Central Alps, Bergell and Adamello, Consiglio Nazionale delle Ricerche, Sienna, Italy, 91–115.

Baumgartner, L. P., and Ferry, J. M. (1991). A model for coupled fluid-flow and mixed-volatile mineral reactions with applications to regional metamorphism. Contributions to Mineralogy and Petrology, 106, 273–285.

Baumgartner, L. P., Michel, J., Putlitz, B., Leuthold, J., Müntener, O., Robyr, M. and Darbellay, B. (2007) Field guide to the Torres del Paine Igneous Complex and its contact aureole. in Field guide book GEOSUR 2007, vol. 185.

Baumgartner, L. P. and Valley, J. W. (2001) Stable Isotope Transport and Contact Metamorphic Fluid Flow. Reviews in Mineralogy and Geochemistry, 43, 415–467.

Bégué, F., Baumgartner, L.P., and Ewing, T. (2018) Density instabilities, melt remobilization and their relationship to volatile exsolution; Torres del Paine igneous complex (Patagonia, Chile). EGU General Assembly Conference Abstracts 20, 12739.

Bickle, M. and J. Baker (1990) Migration of reaction and isotopic fronts in infiltration zones: assessments of fluid flux in metamorphic terrains. Earth and Planetary Science Letters, 98, 1–13.

Bodner, R., Baumgartner, L. P., and Foster, C. T., Jr. (2013). Cordierite nucleation and growth rates in the Torres del Paine contact aureole. Goldschmidt 2013 Conference

Abstracts, 724.

Bowman, J. R., Willett, S. D. and Cook, S. J. (1994) Oxygen isotopic transport and exchange during fluid flow: one-dimensional models and applications. American Journal of Sciences, 294, 1-55.

Candela, P.A. (1986) Toward a thermodynamic model for the halogens in magmatic systems: an application to melt-vapor-apatite equilibria. Chemical Geology, 57, 289–301.

Candela, P. A. (1997). A review of shallow, ore-related granites: Textures, volatiles, and ore metals. Journal of Petrology, 38, 1619–1633.

Cartwright, I., and Buick, I. S. (1996) Determining the direction of contact metamorphic fluid flow: an assessment of mineralogical and stable isotope criteria. Journal of Metamorphic Geology, 14, 289–305.

Connolly, J.A.D. (2009) The geodynamic equation of state: What and how. Geochemistry, Geophysics, Geosystems, 10, Q10014.

Connolly, J. A. D., and Cesare, B. (1993) C-O-H-S fluid composition and oxygen fugacity in graphitic metapelites. Journal of Metamorphic Geology, 11, 379–388.

Cook, S. J., & Bowman, J. R. (1994). Contact metamorphism surrounding the Alta stock: Thermal constraints and evidence of advective heat transport from calcite + dolomite geothermometry. *American Mineralogist*, *79*(5-6), 513–525.

Cook, S. J., Bowman, J. R. and Forster, C. B. (1997) Contact metamorphism surrounding the Alta Stock; finite element model simulation of heat- and $^{18}O/^{16}O$ mass-transport during prograde metamorphism. American Journal of Science, 297, 1–55.

Cui, X. J., Nabelek, P. I., and Liu, M. (2001). Heat and fluid flow in contact metamorphic aureoles with layered and transient permeability, with application to the Notch Peak aureole, Utah. Journal of Geophysical Research, 106, 6477–6491.

Eiler, J.M., Valley, J.W., and Baumgartner, L.P. (1993) A new look at stable isotope thermometry. Geochimica et Cosmochimica Acta, 57, 2571–2583.

Ferry, J. (1986) Reaction Progress: A Monitor of Fluid—Rock Interaction during

Metamorphic and Hydrothermal Events. in Fluid—Rock Interactions during Metamorphism, ed. by J. Walther and B. Wood, Springer New York, vol. 5 of Advances in Physical Geochemistry, 60–88.

Ferry, J.M. (2000) Patterns of mineral occurrence in metamorphic rocks. American Mineralogist, 85, 1573–1588.

Ferry, J.M., Winslow, N.W., and Penniston-Dorland, S.C. (2013) Re-evaluation of Infiltration-driven Regional Metamorphism in Northern New England: New Transport Models with Solid Solution and Cross-layer Equilibration of Fluid Composition. Journal of Petrology, 54, 2455–2485.

Floess, D., Baumgartner, L.P., and Vonlanthen, P. (2015) An observational and thermodynamic investigation of carbonate partial melting. Earth and Planetary Science Letters, 409, 147–156.

Fildani, A. (2005). Stratigraphic record across a retroarc basin inversion: Rocas Verdes–Magallanes Basin, Patagonian Andes, Chile. Geological Society of America Bulletin, 117(11), 1596.

Fildani, A., Schultz, M. R., Graham, S. A., and Leier, A. (2007). A deep-water amalgamated sheet system, Punta Barrosa Formation, Marina's cliff, chile.
In: Nilsen T., Shew R., Steffens G. & Studlick J. (eds.), Atlas of deep-water outcrops. *AAPG Studies in Geology*, vol. 56, p. 125-127.

Gerdes, M. L., Baumgartner, L. P., and Person, M. (1998). Convective fluid flow through heterogeneous country rocks during contact metamorphism. Journal of Geophysical Research: Solid Earth, 103, 23983–24003.

Goranson, R.W. (1983) Silicate-water systems phase equilibria in the $NaAlSi_3O_8$-H_2O and $KAlSi_3O_8$-H_2O systems at high temperatures and pressures. American Journal of Science, 35, 71–91.

Hanson, R. B. (1995) The hydrodynamics of contact metamorphism. Geological Society of America Bulletin, 107, 595–611.

Henry, D.J., and Guidotti, C.V. (2002) Titanium in biotite from metapellitic rocks:

Temperature effect, crystal-chemical controls, and petrologic applications. American Mineralogist, 87, 375–382.

Henry, D. J., Guidotti, C. V. and Thomson, J. A. (2005) The Ti-saturation surface for low-to-medium pressure metapelitic biotites: Implications for geothermometry and Ti-substitution mechanisms. American Mineralogist, 90(2-3), 316–328.

Henry, D.J., and Daigle, N.M. (2018) Chlorine incorporation into amphibole and biotite in high-grade iron-formations: Interplay between crystallography and metamorphic fluids. American Mineralogist, 103, 55–68.

Higashino, F., Kawakami, T., Satish-Kumar, M., Ishikawa, M., Maki, K., Tsuchiya, N., et al. (2013) Chlorine-rich fluid or melt activity during granulite facies metamorphism in the Late Proterozoic to Cambrian continental collision zone—An example from the Sør Rondane Mountains, East Antarctica. Precambrian Research, 234, 229–246.

Holland, T.J.B., and Powell, R. (1991) A Compensated-Redlich-Kwong (CORK) equation for volumes and fugacities of CO_2 and H_2O in the range 1 bar to 50 kbar and 100-1600°C. Contributions to Mineralogy and Petrology, 109, 265–273.

Holness, M. B. (1997). Fluid flow paths and mechanisms of fluid infiltration in carbonates during contact metamorphism: the Beinn an Dubhaich aureole, Skye. *Journal of Metamorphic* Geology, 15(1), 59–70.

Holness, M. B., and Clemens, J. D. (1999). Partial melting of the Appin Quartzite driven by fracture-controlled H 2 O infiltration in the aureole of the Ballachulish Igneous Complex, Scottish Highlands. Contributions to Mineralogy and Petrology, 136, 154–168.

Holtz, F., Behrens, H., Dingwell, D.B., and Johannes, W. (1995) H_2O solubility in haplogranitic metls – compositional, pressure, and temperature-dependance. American Mineralogist, 80, 94–108.

Hubbard, S. M., Romans, B. W., and Graham, S. A. (2008). Deep-water foreland basin deposits of the Cerro Toro Formation, Magallanes basin, Chile: architectural elements of a sinuous basin axial channel belt. Sedimentology, 55(5), 1333–1359.

Icenhower, J.P., and London, D. (1997) Partitioning of fluorine and chlorine between biotite and granitic melt: experimental calibration at 200 MPa H. Contributions to Mineralogy and Petrology, 127, 17–29.

Johannes, W., Holtz, F. (1996) Petrogenesis and experimental petrology of granitic rocks. Springer-Verlag Berlin Heidelberg.

King, P. L., Chappell, B. W., Allen, C. M., & White, A. (2001). Are A-type granites the high-temperature felsic granites? Evidence from fractionated granites of the Wangrah Suite. Australian Journal of Earth Sciences, 48(4), 501–514.

Kretz, R. (1983) Symbols for rock-forming minerals. American Mineralogist, 68, 277–279.

Labotka, T.C., Nabelek, P.I. and Papike, J.J. (1988) Fluid infiltration through the Big Horse Limestone Member in the Notch Peak contact-metamorphic aureole, Utah. American Mineralogist, 73, 1302–1324.

Lacroix, B., and Vennemann, T. (2015) Empirical calibration of the oxygen isotope fractionation between quartz and Fe-Mg-chlorite. Geochimica et Cosmochimica Acta, 149, 21–31.

Leuthold, J. (2011) Geometry, petrology and growth of a shallow crustal laccolith : the Torres del Paine Mafic Complex (Patagonia). Thesis, Université de Lausanne.

Leuthold, J., Müntener, O., Baumgartner, L.P., Putlitz, B. and Chiaradia, M. (2013) A Detailed Geochemical Study of a Shallow Arc-related Laccolith; the Torres del Paine Mafic Complex (Patagonia). Journal of Petrology, 54, 273–303.

Leuthold, J., Müntener, O., Baumgartner, L.P., Putlitz, B., Ovtcharova, M. and Schaltegger, U. (2012) Time resolved construction of a bimodal laccolith (Torres del Paine, Patagonia). Earth and Planetary Science Letters, 325-326, 85–92.

Luisier, C., Baumgartner, L., Siron, G., Vennemann, T., and Robyr, M. (2019) H 2O Content Measurement in Phengite by Secondary Ion Mass Spectrometry: A New Set of Reference Materials. Geostandards and Geoanalytical Research, 43, 635–646.

Luth, W. C., Jahns, R. H., and Tuttle, O. F. (1964) The granite system at pressures of 4 to 10 kilobars. Journal of Geophysical Research, 69, 759–773.

Michel, J., Baumgartner, L. P., Putlitz, B., Schaltegger, U. and Ovtcharova, M. (2008) Incremental growth of the Patagonian Torres del Paine laccolith over 90 k.y. Geology, 36, 459–462.

Müller, T., Baumgartner, L. P., Foster, C. T. and Roselle, G. T. (2008) Forward modeling of the effects of mixed volatile reaction, volume diffusion, and formation of submicroscopic exsolution lamellae on calcite-dolomite thermometry. American Mineralogist 93, 1245–1259.

Munoz, J.L. (1984) F-OH and Cl-OH Exchange in Micas with Applications to Hydrothermal Ore Deposits. Reviews in Mineralogy and Geochemistry, 13, 469–493.

Müntener O., Ewing T. A., Baumgartner L. P., Manzini M., Roux T., Pellaud P. and Alleman L. (2018) Source and fractionation controls on subduction-related plutons and dike swarms in southern Patagonia (Torres del Paine area) and the low Nb/Ta of upper crustal igneous rocks. Contribution to Mineralogy and Petrology, 173, 1–22.

Nabelek, P. I. and Labotka, T. C. (1993). Implications of geochemical fronts in the Notch Peak contact metamorphic aureole, Utah, USA. Earth and Planetary Science Letters. 119, 539–559.

Newton, R. C., Charlu, T. V., & Kleppa, O. J. (1980). Thermochemistry of the high structural state plagioclases. *Geochimica et Cosmochimica Acta*, *44*(7), 933-941.

Pattison, D.R.M., and Tracy, R.J. (1991) Phase equilibria and thermobarometry of metapelites. Reviews in Mineralogy and Geochemistry, 105–206.

Pattison, D. R. M., and Tinkham, D. K. (2009). Interplay between equilibrium and kinetics in prograde metamorphism of pelites: an example from the Nelson aureole, British Columbia. Journal of Metamorphic Geology, 27(4), 249–279.

Powell, R., & Holland, T. (1999). Relating formulations of the thermodynamics of mineral solid solutions; activity modeling of pyroxenes, amphiboles, and micas. *American Mineralogist*, *84*(1-2), 1-14.

Putlitz, B., Baumgartner, L.P., Oberhänsli, R., Diamond, L. and Altenberger, U. (2001) The Torres del Paine Laccolith (Chile); intrusion and metamorphism. LPI Contribution, abstract no. 3534.

Roselle, G.T., Baumgartner, L.P. and Valley, J.W. (1999) Stable isotope evidence of heterogeneous fluid infiltration at the Ubehebe Peak contact aureole, Death Valley National Park, California. American Journal of Science, 299, 93–138.

Sheppard, S.M.F. (1986) Characterization and isotopic variations in natural waters. Reviews in Mineralogy and Geochemistry, 16, 165–184.

Siron, G., Baumgartner, L.P., and Bouvier, A.-S. (2018a) Significance of OH, F and Cl content in biotite during metamorphism of the Western Adamello contact aureole. Contributions to Mineralogy and Petrology, 173, 1–19.

Siron, G., Baumgartner, L.P., Bouvier, A.-S., and Vennemann, T. (2018b) Accurate Measurements of H 2O, F and Cl Contents in Biotite Using Secondary Ion Mass Spectrometry. Geostandards and Geoanalytical Research, 363, 229–16.

Sisson V. B. (1987) Halogen chemistry as an indicator of metamorphic fluid interaction with the Ponder pluton, Coast Plutonic Complex, British Columbia, Canada. Contribution to Mineralogy and Petrology, 95, 123–131.

Smye, A.J., Bickle, M.J., Holland, T.J.B., Parrish, R.R., and Condon, D.J. (2011) Rapid formation and exhumation of the youngest Alpine eclogites: A thermal conundrum to Barrovian metamorphism. Earth and Planetary Science Letters, 306, 193–204.

Spear, F.S. (1993) Metamorphic Phase Equilibria and Pressure-Temperature Paths, *Mineralogical Society of America, Washington D.C.*, 799 p.

Speer, A.J. (1984) Micas in Igneous Rocks. Reviews in Mineralogy and Geochemistry, 13, 299–356.

Süssenberger, A., Schmidt, S.T., Wemmer, K., Baumgartner, L.P., and Grobety, B. (2017) Timing and thermal evolution of fold-and-thrust belt formation in the Ultima Esperanza District, 51°S Chile: Constraints from K-Ar dating and illite characterization. Geological Society of America Bulletin, 130, 975–998.

Suzuoki, T. and Epstein, S. (1976) Hydrogen isotope fractionation between OH-bearing minerals and water. Geochimica and Cosmochimica Acta, 40, 1229–1240.

Tajčmanová, L., Connolly, J.A.D., and Cesare, B. (2009) A thermodynamic model for titanium and ferric iron solution in biotite. Journal of Metamorphic Geology, 27, 153–165.

Tuttle, O. F., and Bowen, N. L., 1958, Origin of granite in the light of experimental studies in the system $NaAlSi_3O_8$-$KAlSi_3O_8$-SiO_2-H_2O: Geological Society of America Memoir 74, 153 p.

Waldbaum, D. R., & Thompson, J. B. (1968). Mixing Properties Of Sanidine Crystalline Solutions .2. Calculations Based On Volume Data. *American Mineralogist*, 2000-2017.

Waters, D. J., and Lovegrove, D. P. (2002). Assessing the extent of disequilibrium and overstepping of prograde metamorphic reactions in metapelites from the Bushveld Complex aureole, South Africa. Journal of Metamorphic Geology, 20, 135–149.

Webster, J.D., Vetere, F., Botcharnikov, R.E., Goldoff, B., McBirney, A., and Doherty, A.L. (2015) Experimental and modeled chlorine solubilities in aluminosilicate melts at 1 to 7000 bars and 700 to 1250 °C: Applications to magmas of Augustine Volcano, Alaska. American Mineralogist, 100, 522–535.

Wilson, T.J. (1991) Transition from back-arc to foreland basin development in the southernmost Andes: Stratigraphic record from the Ultima Esperanza District, Chile. Geological Society of America Bulletin, 103, 98–111.

White, R. W., Pomroy, N. E., & Powell, R. (2005). An in situ metatexite–diatexite transition in upper amphibolite facies rocks from Broken Hill, Australia. *Journal of Metamorphic Geology*, *23*(7), 579-602.

Zhu, C. and Sverjensky, D.A. (1991) Partitioning of F-Cl-OH between minerals and hydrothermal fluids. Geochimica Et Cosmochimica Acta, 55, 1837–1858.

Zhu, C., and Sverjensky, D.A. (1992) F-Cl-OH partitioning between biotite and apatite. Geochimica et Cosmochimica Acta, 56, 3435–3467.

APPENDIX

All pseudosections were computed using the 2002 version of the Holland and Powell (1998) thermodynamic database (hp02ver in Perple_X). Activity-composition models used for each mineral for thermodynamic modelling are as follow:

- Biotite: Bio(TCC), Tajcmanova et al. (2009)
- White mica: Mica(SGH), Smye et al. (2011)
- Plagioclase: Pl(h), Newton et al. (1980)
- Orthoclase: San, Waldbaum and Thompson (1968)
- Chloritoid: Ctd(SGH), Smye et al. (2011)
- Cordierite: hCrd, White et al. (2005)
- Chlorite: Chl(SGH), Smye et al. (2011)
- Staurolite: St(HP), Powell and Holland (1999)

Figure Captions

Figure 1: (a) Geological map of the Torres del Paine Intrusion (TPI); The TPIC has a west-east and a North-South extension of about 12 and 8 km, respectively. The TPI is a bimodal laccolith which consists of three older granitic (12.59-12.50 Ma, Michel et al. 2008; Leuthold et al., 2012), an older mafic unit (12.6Ma) and three youngers mafic (12.5-12.43 Ma, Leuthold et al. 2012) pulses. It intruded into the sediments of the Punta Barrosa and Cerro Toro formations. The investigated localities are situated in the Cerro Toro formation (black stars). (b) A profile above and below the intrusion was investigated at the Cuerno Principal, at the south end of the TPI. The thickness of the contact aureole is indicated by the perpendicular white line. It is 400 and 150 m below and above the intrusion, respectively. (c) The thickness of the contact aureole at the investigated profile on the Cerro Fortaleza is larger than what was collected, because the summit still contains cordierite. The thickness from the

upper contact to the summit is 260 m. At the Fortaleza the intrusion is thicker than at the other profile localities. It is at least 1.5 km thick; the bottom of the intrusion is not exposed. (d) The Monte Almirante is situated at the east end of the laccolith. This represents the front end of the magma injection (Baumgartner et al., 2007). One profile above the intrusion was investigated. The contact aureole thickness is 200 m. (e) The profile in the Valle Frances is situated at the side of the intrusion. The thickness of the contact aureole is approximately 200m, measured perpendicular to the subvertical contact. (b)-(e) Abbreviations: CPa (Cuerno Principal above), CPb (Cuerno Principal below), F (Fortaleza), A (Almirante) and VF (Valle Frances).

Figure 2: BSE images of different samples of the Torres del Paine contact aureole showing textural change during metamorphism and fluid infiltration; a) big grains of detritic quartz (qtz) and metamorphic cordierite (crd). The sample 07TP56 is located at 300m from the contact; b) detritic muscovite in sample 07TP55 at 400m from the contact; c) The decrease in grain size of cordierite and quartz is well shown in this image from sample 07TP58 at 150m from the contact; d) Altered cordierite, which is dissolved along grain boundaries (crd’) is shown in this image from sample 12P22, located at the contact. Abundant retrogression of cordierite and biotite to chlorite + muscovite (chl+ms) is shown. Plagioclase (pl) and quartz (qtz) are equigranular and homogeneously distributed in the rock; e) retrograde muscovite is present in sample 10TP57 collected at the contact with the intrusion. Note that biotite from this sample has the highest Cl content. Biotite has well defined, straight grain boundaries and is more homogeneously distributed at the thin section scale; f) chlorite + muscovite intergrowth in sample 10TP54, collected at 1m from the contact. Note that this sample contains low chlorine content biotite. Mineral abbreviations after Kretz (1983).

Figure 3: Biotite compositions from the profile below the intrusion at the Cuerno Principal location; a) There are two different Ti vs X_{Mg} different trends defined by the data: biotites with low Cl content show relatively low X_{Mg} -values, while samples close to the contact have higher X_{Mg} values. In either case, the X_{Mg} values decrease with increasing Ti with increasing temperature, and the high Cl content at higher X_{Mg}; b) Cl content in biotite plotted against the distance from the intrusion. No trend in chlorine content is observed for most samples. Only two samples in the immediate vicinity of the intrusion show high chlorine concentrations reflecting igneous fluid infiltration.

Figure 4: AFM triangular plot of all the bulk rock composition from the Torres del Paine contact aureole (n=71). The diagram was constructed by projecting from muscovite, quartz, and fluid. The FeO content was corrected for ilmenite, the major Ti oxide phase found in these rocks. White symbol represents the bulk rock composition (sample 07TP56) chosen for thermodynamic modeling.

Figure 5: a) T-X_{Mg} pseudosection was calculated for the bulk composition of sample 07TP56 by keeping the measured sum of FeO+MgO constant, but varying X_{Mg}. The dark grey range outlines the variation of composition for the Torres del Paine rocks. The hatched area represent the stability field of andalusite; b) P-T pseudosection for the composition of 07TP56, x-axis is shared with c); a) and b) are projected through ilmenite and graphite, fields correspond to 1) Chl + Ms + Crd, 2) Chl + Ms + Crd + Bt, 3) Ms + Crd + Bt + Kfs; c) Modes for the major minerals in the Torres del Paine contact aureole at 750 bars, the major isograds are highlighted in grey (crd+, bt+, Chl-, Kfs+ and Ms-).

Figure 6: Fluid infiltration textures seen in the field are restricted to localized fractures and dykes. a) Many dykes emanate from the roof and the distal parts of the Torres del Paine intrusion. Here an image of a typical dyke emanating from the frontal part into the host rocks in the Co. Almirante Nieto area. Note that the dykes split up into a myriad of dyklets. Each dykelet transitions into a veinlet, which can be followed for about 10m. These horse-tail like dykes are common around the intrusion. See also Müntener et al. (2018). b) Bleaching zones at the contact and surrounding dyklets are common. They are typically only a few 10's of centimeters wide.

Figure 7: Bulk rock isotopic measurements are shown, with symbols keyed to the different profiles. a) Oxygen isotope compositional variations are small, and do not show any conclusive trends with respect to distance to the intrusion b) Hydrogen isotope vary systematically as a function to the distance of the intrusion in all profiles. Compositions first decrease towards the intrusion and slightly increase towards the contact. See text for more details.

Figure 8: Cl content in metamorphic biotite from the contact aureole plotted against distance from the intrusion for the 5 studied profiles; a) Cuerno Princiapl below (CPb) profile; b) Cuerno Principal above (CPa) profile; c) Mte. Almirante profile; d) Fortaleza profile; e) Valle Frances profile; f) Average Cl content distribution in the contact aureole for the 5 profiles studied, symbols are the same as in panels a), b), c) d), e). Note that chlorine concentration is low in the far-field of the aureole in all samples, while some samples show elevated concentrations of chlorine close to the contact. Note however, that not all samples in the proximity of the contact are elevated.

Figure 9: Cl content in metamorphic biotite in the contact aureole plotted against X_{Mg} composition for the 5 studied profiles; a) Cuerno Princiapl below (CPb) profile; b) Cuerno Principal above (CPa) profile; c) Mte. Almirante profile; d) Fortaleza profile; e) Valle Frances profile; f) Average Cl content vs X_{Mg} for all profiles, symbols are the same as in panels a), b), c) d), e). No correlation between X_{Mg} and Cl content in biotite can be found, in contradiction with the Mg-Cl avoidance rule.

Figure 10: Schematic temperature-time evolution diagram showing the fluid infiltration events for samples located close to the contact of the intrusion. The suggested relative fluid infiltration events are shown with bold lines. Note that high salinity fluids from the intrusions infiltrated the metapelites post-peak, but still in the stability field of biotite and likely K-feldspar. Subsequent infiltration produced first retrograde, coarse muscovite, then fine grained muscovite and chloride in the pinitized cordierites. While fluid infiltration is shown as discrete events, fluid infiltration might have been continuous in time, but localized in space.

Table 1: major element compositions of mucovite from the Cuerno Principal below gradient, Structural formulae are computed using 44 charges or 22 equivalent oxygens.

	Muscovite				
	07TP55	1sd	07TP56	1sd	07TP58
SiO_2	49.79	(5.66)	49.01	(1.51)	47.19
TiO_2	0.1	(0.17)	0.16	(0.09)	0.34
Al_2O_3	32.82	(5.39)	32.66	(2.06)	36.15
FeO	1.87	(1.19)	2.03	(0.47)	0.99
MgO	1.42	(1.45)	1.46	(0.38)	0.52
MnO	0.01	(0.02)	0.01	(0.01)	0.01
CaO	0.08	(0.17)	0.13	(0.31)	0.02
K_2O	8.84	(1.19)	8.74	(0.61)	9.41
Na_2O	0.54	(0.39)	0.79	(0.61)	0.48
F	0.06	(0.08)	0.05	(0.02)	0.04
Cl	b.d.l.		b.d.l.		b.d.l.
O = F	0.02	(0.03)	0.02	(0.01)	0.02
Total	95.51	(1.48)	95.02	(0.7)	95.14
Al^{tot}	5.076	(0.854)	5.091	(0.633)	5.617
Si	6.531	(0.626)	6.481	(0.363)	6.219
^{IV}Al	1.469	(0.626)	1.519	(0.363)	1.781
Sum	8		8		8
^{VI}Al	3.607	(0.323)	3.572	(0.285)	3.836
Fe	0.206	(0.133)	0.224	(0.107)	0.11
Mg	0.278	(0.287)	0.289	(0.152)	0.102
Mn	0.001	(0.002)	0.001	(0.003)	0.001
Ti	0.01	(0.017)	0.015	(0.017)	0.034
Sum	4.102	(0.175)	4.102	(0.176)	4.082
K	1.48	(0.218)	1.474	(0.209)	1.583
Na	0.069	(0.049)	0.101	(0.156)	0.062
Ca	0.011	(0.023)	0.019	(0.087)	0.003
Sum	1.559	(0.225)	1.594	(0.072)	1.648
F	0.025	(0.033)	0.023	(0.02)	0.018
Cl	b.d.l.		b.d.l.		b.d.l.
X_{Mg} [a]	0.549	(0.165)	0.559	(0.08)	0.48
$^{VI}R^{2+} / (^{VI}R^{2+} + ^{VI}R^{3+})$	0.118	(0.097)	0.126	(0.060)	0.052

Distance (m)	400	300	150
Estimated T (°C) [b]	470	490	510

[a] compute as follow : X_{Mg} = Mg / (Mg + Fe)

[b] Estimated from phase petrology and distance from the contact

b.d.l. : below detection limit

determined by electron microprobe.

1sd	10TP54	1sd	10TP57	1sd
(1.33)	49.83	(6.37)	47.43	(1.14)
(0.31)	0.04	(0.05)	0.03	(0.1)
(0.7)	34.87	(5.76)	35.76	(1.23)
(0.2)	1.26	(0.28)	1.29	(0.48)
(0.12)	0.63	(0.09)	0.91	(0.28)
(0.01)	0.02	(0.02)	0.02	(0.02)
(0.02)	0.02	(0.02)	0	(0.01)
(0.69)	8.95	(2.1)	10.22	(0.26)
(0.04)	0.54	(0.33)	0.48	(0.05)
(0.03)	0.06	(0.09)	0.08	(0.05)
	b.d.l.		b.d.l.	
(0.01)	0.02	(0.04)	0.03	(0.02)
(1.24)	96.2	(1.35)	96.18	(2.13)
(0.2)	5.332	(0.934)	5.536	(0.087)
(0.225)	6.46	(0.704)	6.221	(0.046)
(0.225)	1.54	(0.704)	1.779	(0.046)
	8		8	
(0.085)	3.792	(0.246)	3.756	(0.065)
(0.047)	0.137	(0.027)	0.152	(0.034)
(0.049)	0.122	(0.017)	0.181	(0.066)
(0.002)	0.002	(0.002)	0.002	(0.002)
(0.062)	0.004	(0.005)	0.003	(0.011)
(0.05)	4.057	(0.211)	4.094	(0.026)
(0.239)	1.483	(0.386)	1.703	(0.055)
(0.011)	0.068	(0.04)	0.062	(0.003)
(0.005)	0.003	(0.002)	0.001	(0.002)
(0.235)	1.554	(0.351)	1.765	(0.053)
(0.024)	0.018	(0.039)	0.03	(0.017)
	b.d.l.		b.d.l.	
(0.048)	0.472	(0.042)	0.543	(0.044)
(0.022)	0.065	(0.013)	0.082	(0.023)

5	1
590	600

Table 3: representative major element compositions of feldspars from the Cuerno Principal below gradie

	Plagioclases					
	07TP56		07TP58		07TP63	
	low X_{An}	high X_{An}	low X_{An}	high X_{An}	low X_{An}	high X_{An}
SiO_2	68.81	61.03	66.69	64.50	59.60	49.16
TiO_2	0.02	0.01	0.01	0.01	0.00	0.02
Al_2O_3	19.97	23.93	20.92	22.40	25.49	32.68
MgO	0.00	0.01	0.00	0.00	0.00	0.00
FeO	0.27	0.25	0.27	0.28	0.28	0.29
CaO	0.31	5.76	2.08	3.56	7.52	16.11
K_2O	0.03	0.06	0.14	0.17	0.06	0.06
Na_2O	11.92	8.58	10.77	9.80	7.39	2.40
Total	101.33	99.62	100.88	100.71	100.35	100.76
Si	2.974	2.726	2.910	2.831	2.652	2.235
Al	1.017	1.260	1.076	1.159	1.337	1.751
Sum	3.992	3.985	3.985	3.990	3.989	3.985
Na	0.999	0.743	0.911	0.834	0.638	0.212
Ca	0.014	0.276	0.097	0.167	0.359	0.785
K	0.002	0.003	0.009	0.010	0.004	0.003
Sum	1.015	1.022	1.017	1.011	1.000	0.999
X_{An} [a]	0.014	0.270	0.096	0.166	0.359	0.786
X_{Ab} [b]	0.984	0.727	0.896	0.825	0.638	0.212
X_{Or} [c]	0.002	0.003	0.008	0.010	0.004	0.003
Distance (m)	300	300	150	150	10	10
Estimated T (°C) [d]	480	480	510	510	560	560

[a] Compute as follow: Ca / (Na + Ca + K)

[b] Compute as follow: Na / (Na + Ca + K)

[c] Compute as follow: K / (Na + Ca + K)

[d] Estimated from phase petrology and thermodynamic modelling

ent, determined by EPMA.

	K-feldspars		
10P54	07TP58	10TP54	10TP57
62.84	65.16	65.18	65.18
0.03	0	0	0
23.01	18.45	18.44	18.59
0.01	0.0612	0.0084	0.0145
0.22	0.4052	0.3017	0.1368
4.70	0.0127	0.0261	0.028
0.19	11.99	13.85	14.05
9.25	2.45	1.74	1.83
100.25	98.5396	99.5485	99.8904
2.782	3.006	3.001	2.994
1.200	1.003	1.001	1.007
3.982	4.009	4.001	4.001
0.794	0.219	0.155	0.163
0.223	0.001	0.001	0.001
0.011	0.765	0.882	0.893
1.028	0.985	1.039	1.058
0.217	0.001	0.001	0.001
0.772	0.222	0.149	0.154
0.011	0.777	0.849	0.845
5	150	5	1
570	510	590	600

Table 3 : major element compositions of biotite from the Cuerno Principal below gradient, d

	Biotite				
	07TP55	1sd	07TP56	1sd	07TP58
SiO_2	35.92	(3.81)	35.06	(1.1)	35.15
TiO_2	1.4	(0.2)	1.98	(0.58)	2.75
Al_2O_3	20.08	(1.24)	19.68	(0.95)	20.08
FeO	21.58	(0.96)	21.94	(0.76)	21.41
MgO	7.71	(0.43)	7.45	(0.53)	6.93
MnO	0.06	(0.03)	0.07	(0.03)	0.07
CaO	0.03	(0.1)	0.03	(0.06)	0.16
K_2O	7.86	(0.52)	7.77	(0.64)	8.27
Na_2O	0.13	(0.06)	0.19	(0.2)	0.1
F	0	(0)	0	(0)	0
Cl	0.01	(0.01)	0.01	(0.01)	0.02
O = F	0	(0)	0	(0)	0
Total	94.79	(1.25)	94.18	(1.36)	94.94
Al^{tot}	3.612	(0.301)	3.578	(0.136)	3.621
Si	5.477	(0.414)	5.409	(0.104)	5.378
^{IV}Al	2.523	(0.414)	2.591	(0.104)	2.622
Sum	8		8		8
^{VI}Al	1.09	(0.139)	0.987	(0.136)	0.999
Fe	2.754	(0.179)	2.831	(0.132)	2.74
Mg	1.753	(0.135)	1.715	(0.129)	1.581
Mn	0.008	(0.004)	0.009	(0.004)	0.01
Ti	0.161	(0.026)	0.231	(0.069)	0.316
Sum	5.765	(0.187)	5.773	(0.141)	5.646
K	1.53	(0.132)	1.53	(0.12)	1.614
Na	0.019	(0.01)	0.028	(0.029)	0.015
Ca	0.006	(0.016)	0.006	(0.009)	0.027
Sum	1.555	(0.139)	1.563	(0.12)	1.656
F	0	(0)	0	(0)	0
Cl	0.002	(0.001)	0.003	(0.003)	0.004
X_{Mg} [a]	0.389	(0.009)	0.377	(0.015)	0.366
Distance (m)	400		300		150

Ti-in biotite T (°C) [b]	512	593	648
Estimated T (°C) [c]	470	490	510

[a] compute as follow : X_{Mg} = Mg / (Mg + Fe)

[b] Computed from biotite composition using the Ti-in biotite geothermometer from Henry et

[c] Estimated from phase petrology and distance from the contact

etermined by electron microprobe.

1sd	07TP63	1sd	10TP54	1sd	10TP57	1sd
(1.42)	35.92	(0.55)	35.67	(0.77)	35.84	(1.56)
(1.39)	1.71	(0.18)	4.04	(0.81)	3.39	(0.62)
(1.11)	17.51	(0.77)	18.48	(0.57)	18.57	(1.34)
(1.13)	21.03	(0.4)	21.83	(0.67)	20.52	(0.9)
(0.71)	9.9	(0.75)	6.74	(0.63)	7.85	(0.41)
(0.03)	0.18	(0.03)	0.1	(0.03)	0.19	(0.09)
(1.22)	0.07	(0.09)	0.05	(0.11)	0.01	(0.02)
(0.46)	9.16	(0.34)	9	(0.28)	9.36	(0.25)
(0.05)	0.11	(0.06)	0.16	(0.33)	0.1	(0.04)
(0)	0	(0)	0	(0)	0.03	(0.08)
(0.01)	0.16	(0.02)	0.01	(0.01)	0.18	(0.02)
(0)	0	(0)	0	(0)	0.01	(0.04)
(2.12)	95.76	(0.88)	96.09	(0.9)	96.03	(1.07)
(0.18)	3.155	(0.131)	3.317	(0.099)	3.328	(0.218)
(0.111)	5.491	(0.059)	5.434	(0.076)	5.448	(0.146)
(0.111)	2.509	(0.059)	2.566	(0.076)	2.552	(0.146)
	8		8		8	
(0.233)	0.646	(0.124)	0.751	(0.125)	0.775	(0.209)
(0.161)	2.689	(0.061)	2.781	(0.094)	2.609	(0.149)
(0.176)	2.257	(0.169)	1.531	(0.152)	1.779	(0.114)
(0.004)	0.023	(0.004)	0.013	(0.004)	0.024	(0.011)
(0.157)	0.197	(0.022)	0.463	(0.092)	0.388	(0.074)
(0.141)	5.812	(0.046)	5.539	(0.122)	5.576	(0.092)
(0.077)	1.786	(0.062)	1.75	(0.055)	1.816	(0.066)
(0.008)	0.017	(0.01)	0.023	(0.047)	0.015	(0.007)
(0.204)	0.012	(0.015)	0.007	(0.017)	0.002	(0.003)
(0.201)	1.815	(0.058)	1.78	(0.035)	1.833	(0.066)
(0)	0	(0)	0	(0)	0.001	(0.004)
(0.003)	0.041	(0.005)	0.003	(0.002)	0.046	(0.006)
(0.033)	0.456	(0.021)	0.355	(0.022)	0.405	(0.013)
	10		5		1	

	575	706	686
	580	590	600

al. (2005)

Table 5: Representative cordierite major element compositions (wt%) from lower profile of Cuerno Principal (CPb)

	07TP55	07TP56	07TP58	10TP54
SiO_2	49.53	48.47	48.92	48.59
TiO_2	0.02	0.01	0.03	0.01
Al_2O_3	31.89	32.43	32.92	32.66
MgO	6.71	6.79	6.5	6.62
FeO	10.25	10.43	11.35	10.88
MnO	0.24	0.24	0.21	0.28
CaO	0.08	0.05	0.02	0.02
Na_2O	0.34	0.28	0.18	0.18
K_2O	0.05	0.04	0.03	0
Cl	0	0	0.01	0.01
Total	99.11	98.73	100.17	99.26
Si	5.103	5.024	5.013	5.017
Al	3.873	3.961	3.976	3.974
Mg	1.031	1.049	0.993	1.019
Fe	0.883	0.904	0.973	0.939
Mn	0.021	0.021	0.018	0.025
Ca	0.009	0.005	0.002	0.003
Na	0.067	0.056	0.036	0.036
K	0.006	0.005	0.004	0
Cl	0	0	0.001	0.002
X_{Mg} [a]	0.539	0.537	0.505	0.52
Distance (m)	400	300	150	5
Estimated T (°C) [b]	470	490	510	590

[a] Compute as follow : $X_{Mg} = Mg /(Mg + Fe)$

[b] Estimated from phase petrology and distance from the contact

Table 5: Isotopic compositions for whole rock granites, quartz and biotites from granite and quartz from miaroles

		^{18}O	δD
Granites	Whole rock	7.1 - 9.1 ‰	
	Quartz	9.1 - 9.9 ‰	
	Biotite	5.1 - 6.0 ‰	-97 to -95 ‰ -88 to -83 ‰
Quartz from cavities		8.8 - 11.1 ‰	

Table 6: bulk rock isotopic measurements in the Torres del Paine aureole

Sample	Profile	distance	^{18}O (‰)	δD (‰)
09TP6	A	1	9.73	-90.38
09TP9	A	3	12.83	-93.31
09TP11	A	35	13.63	-81.84
09TP13	A	75	13.31	-86.69
09TP14	A	100	13.65	-95.39
09TP15	A	120	12.89	-103.29
09TP18	A	150	13.28	-101.26
09TP19	A	180	13.56	-93.34
09TP22	A	250	11.13	-82.39
10P55	A*	40	-	-95.24
07TP63	CPb	10	13.92	-82.13
07TP60	CPb	50	14.67	-85.13
07TP59	CPb	120	14.53	-89.21
07TP58	CPb	150	14.43	-85.93
07TP56	CPb	300	14.51	-78.72
07TP55	CPb	400	15.02	-76.92
07TP54	CPb	520	14.61	-
07TP45	CPb	520	15.06	-79.74
07TP53	CPb	600	14.74	-71.92
07TP48	CPb	670	14.79	-75.71
07TP52	CPb	700	14.49	-73.11
10P103	CPa	2	11.94	-85.83
10P105	CPa	2	12.98	-94.15
10P111	CPa	2	9.92	-110.76
10P84	CPa	2	13.11	-97.24
10P72	CPa	10	13.02	-94.49
10P78	CPa	10	13.8	-90.01
10P91	CPa	23	14.09	-85.49
10P95	CPa	30	13.36	-84.47
10P86	CPa	80	-	-98.14
10P99	CPa	155	10.77	-90.92
10P101	CPa	215	11.21	-91.08
10P144	F	1	23.11	-97.32
10P142	F	8	13.15	-95.41
10P140	F	26	13.22	-94.4
10P138	F	40	13.18	-101.72
10P134	F	80	12.21	-102.78
10P130	F	130	13.14	-93.39

10P120	F	200	13.75	-90.01
10P118	F	230	13.38	-85.54
10P114	F	265	13.42	-96.73
L5	S	>1500	15.08	-80.77
L2A	S	>1500	14.86	-86.64
L17	S	>1500	12.68	-75.41
L12	S	>1500	13.27	-88.33
L20	S	>1500	13.47	-78.94
L23	S	>1500	13.44	-89.32
L31	S	>1500	13.15	-78.03
L40	S	>1500	-	-75.08

Profiles: A = Almirante; A* = Almirante samples with a small offset from regular profile; CPb = Cuerno Principale below; CPa = Cuerno Principale above; F = Fortalezza

Figure 1

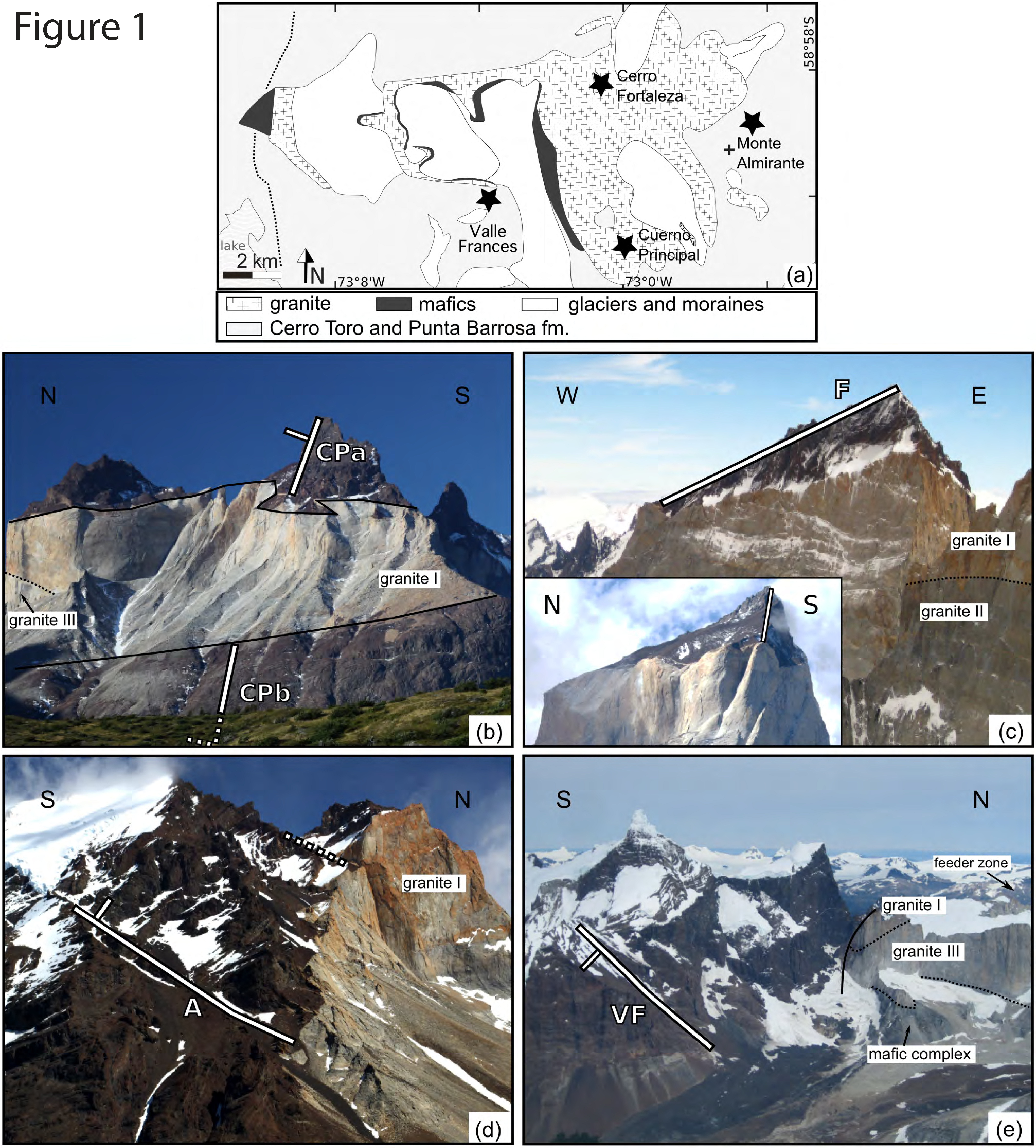
58°58'S
Cerro Fortaleza
Monte Almirante
Valle Frances
Cuerno Principal
lake
2 km
N
73°8'W
73°0'W
(a)
granite
mafics
glaciers and moraines
Cerro Toro and Punta Barrosa fm.
N
S
CPa
granite I
granite III
CPb
(b)
W
F
E
granite I
granite II
N
S
(c)
S
N
granite I
A
(d)
S
N
feeder zone
granite I
granite III
VF
mafic complex
(e)

Figure 2

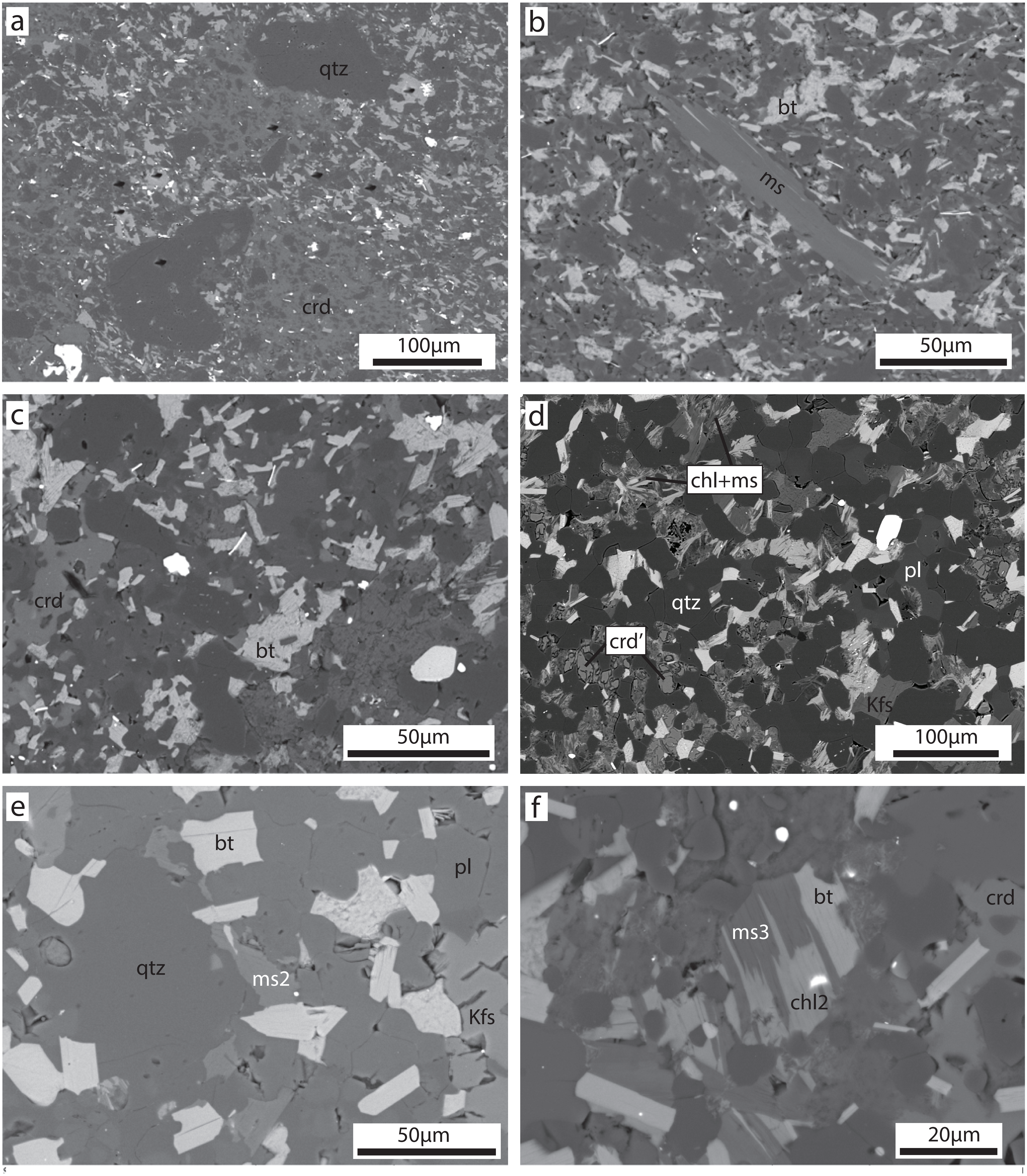
a
qtz
crd
100µm
b
bt
ms
50µm
c
crd
bt
50µm
d
chl+ms
pl
qtz
crd′
Kfs
100µm
e
bt
pl
qtz
ms2
Kfs
50µm
f
bt
crd
ms3
chl2
20µm

Figure 3

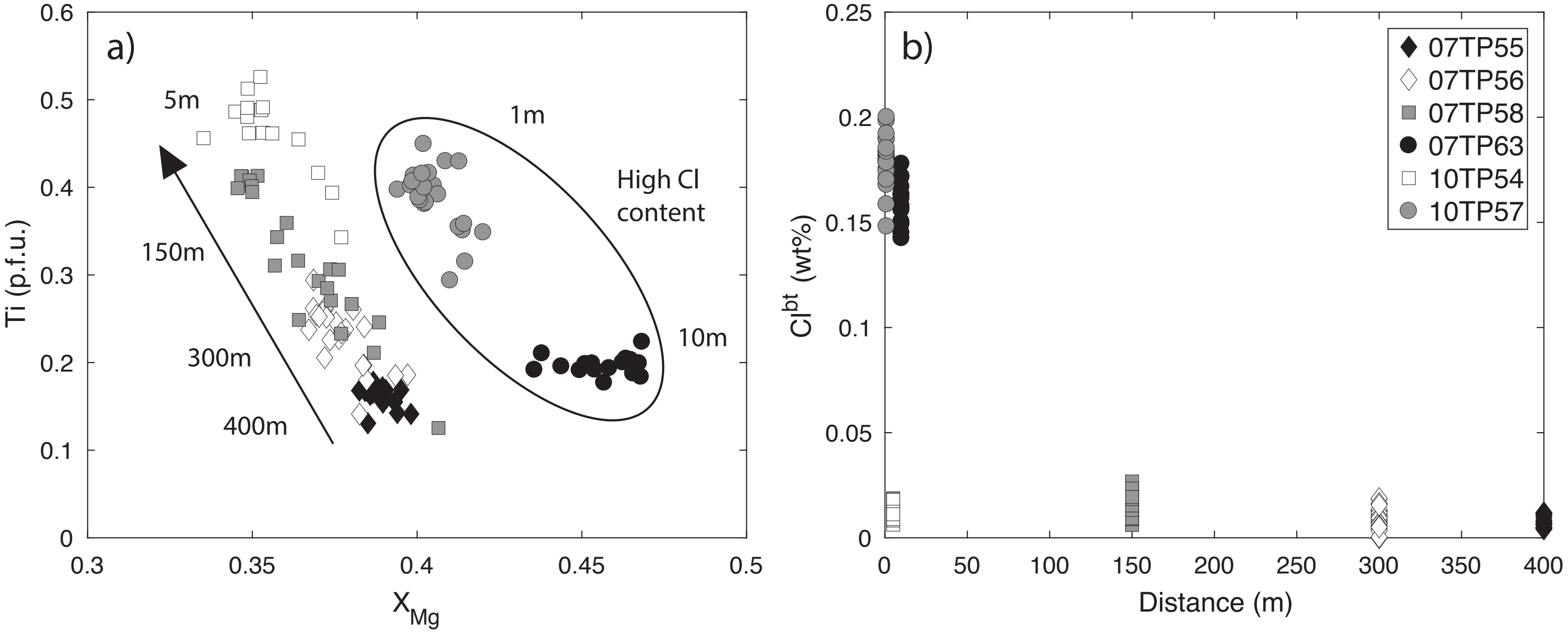

a)
Ti (p.f.u.)
X$_{Mg}$
0.6
0.5
0.4
0.3
0.2
0.1
0
0.3
0.35
0.4
0.45
0.5
5m
150m
300m
400m
1m
High Cl content
10m
b)
Cl^{bt} (wt%)
Distance (m)
0.25
0.2
0.15
0.1
0.05
0
0
50
100
150
200
250
300
350
400
◆ 07TP55
◇ 07TP56
■ 07TP58
● 07TP63
□ 10TP54
● 10TP57

Figure 4

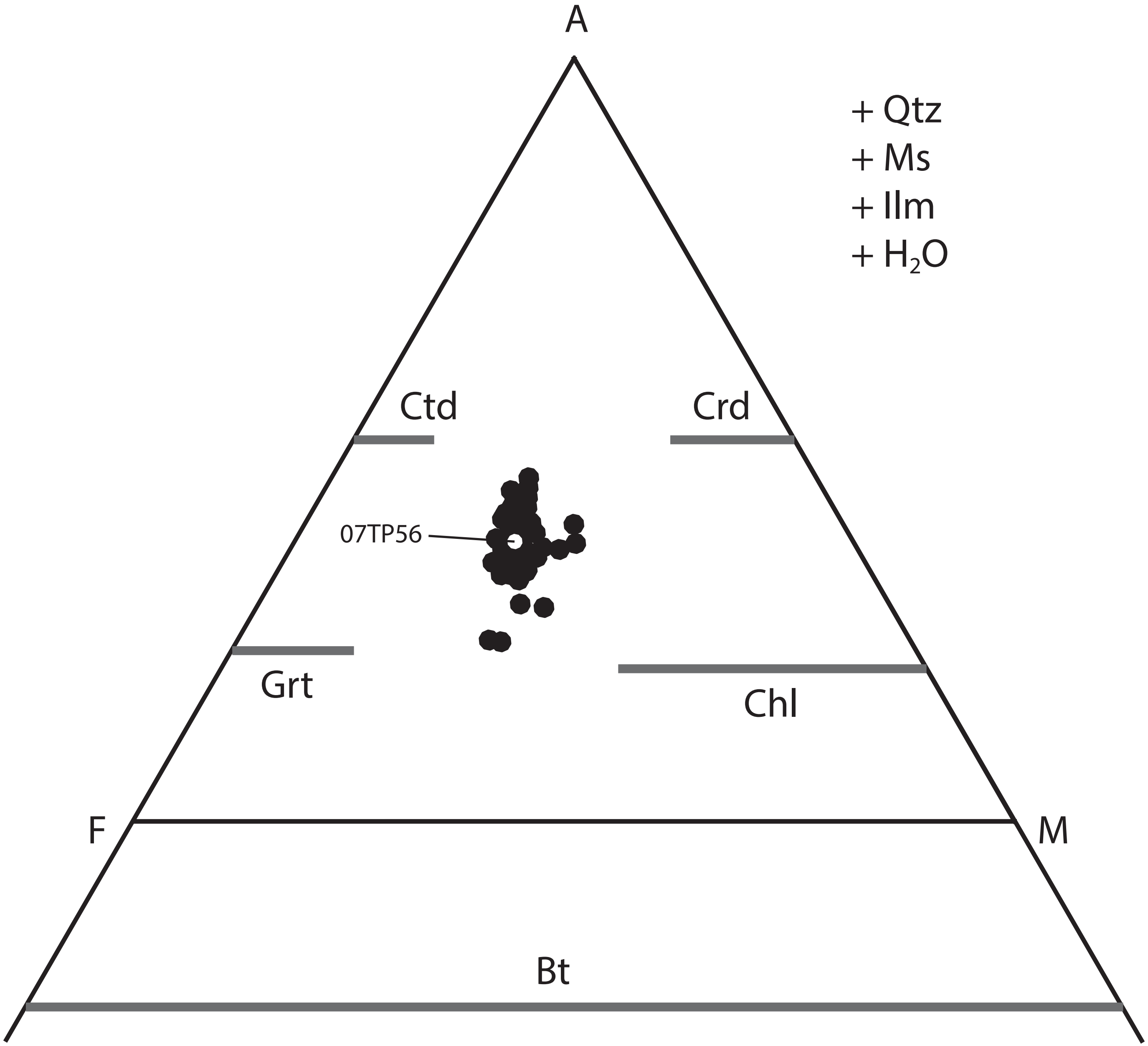

Figure 5

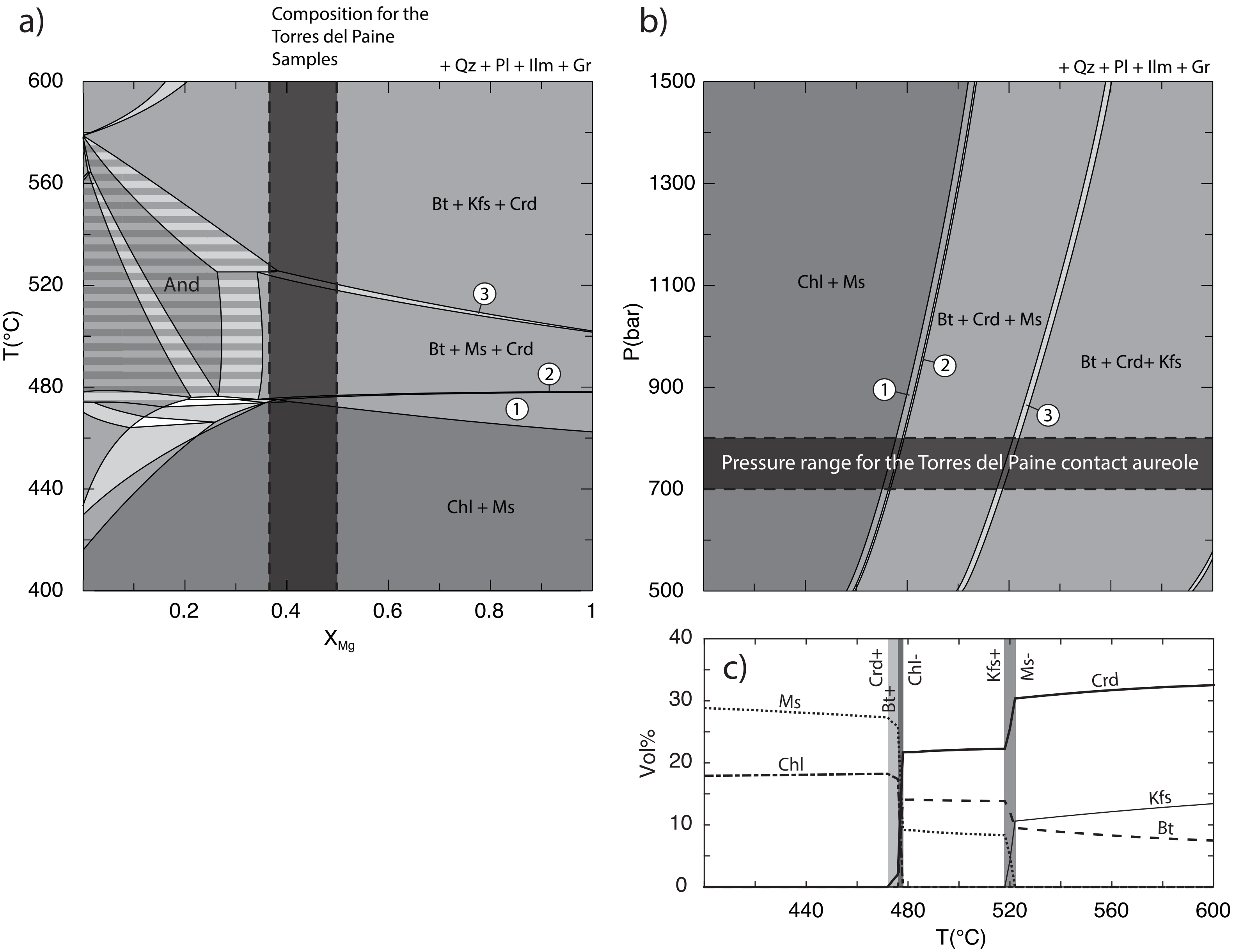
a)
Composition for the Torres del Paine Samples
+ Qz + Pl + Ilm + Gr
600
560
520
480
440
400
T(°C)
Bt + Kfs + Crd
And
③
Bt + Ms + Crd
②
①
Chl + Ms
0.2
0.4
0.6
0.8
1
X$_{Mg}$
b)
+ Qz + Pl + Ilm + Gr
1500
1300
1100
900
700
500
P(bar)
Chl + Ms
Bt + Crd + Ms
Bt + Crd+ Kfs
②
①
③
Pressure range for the Torres del Paine contact aureole
c)
40
30
20
10
0
Vol%
Crd+
Bt+
Chl-
Kfs+
Ms-
Ms
Chl
Crd
Kfs
Bt
440
480
520
560
600
T(°C)

Figure 6

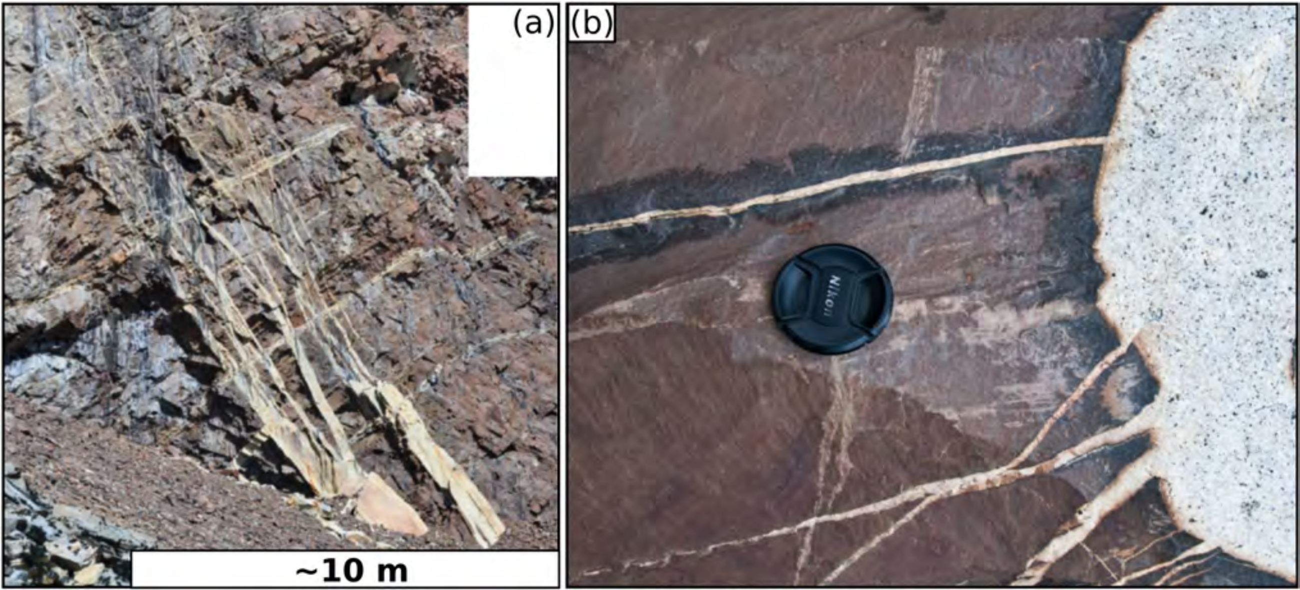

Figure 7

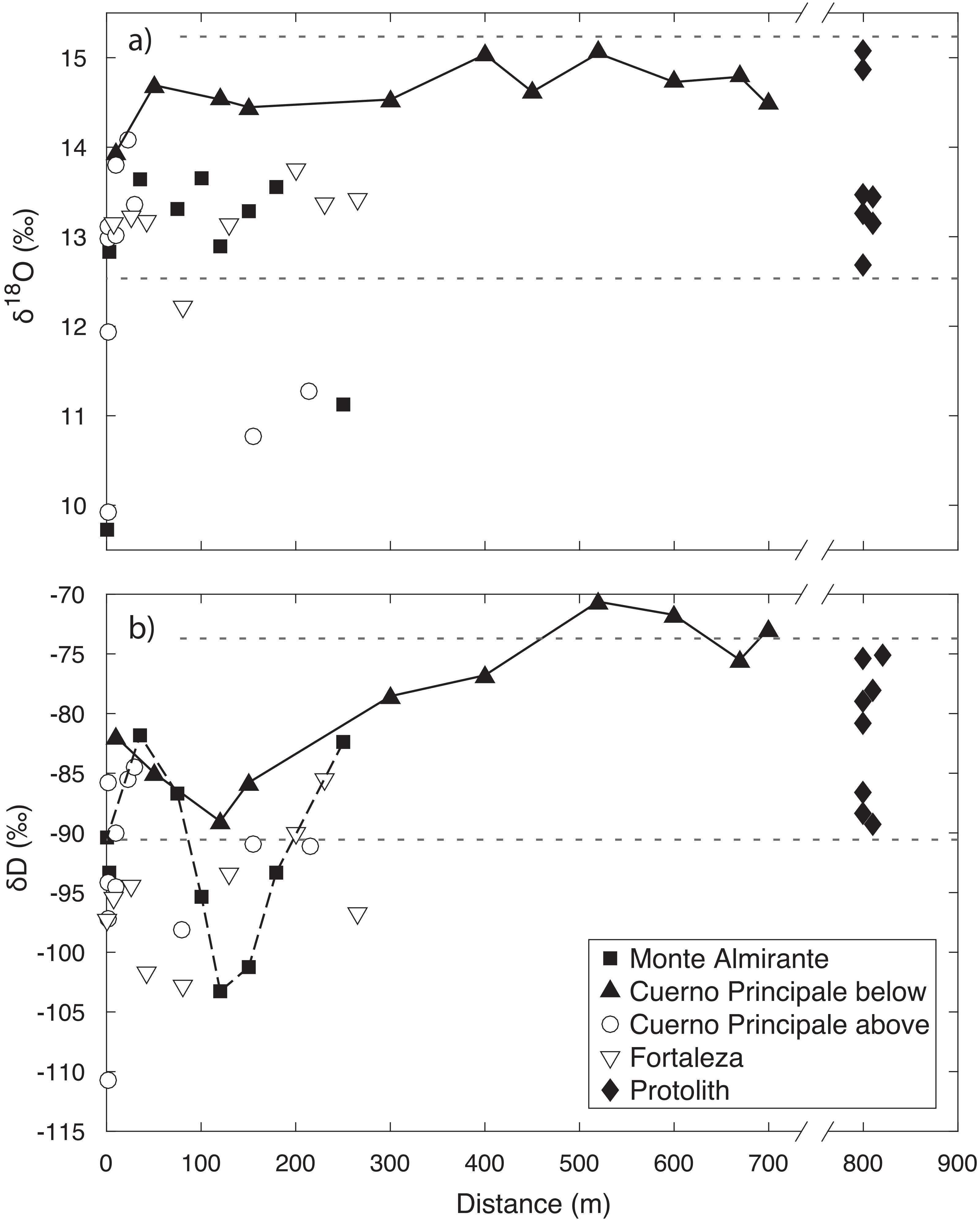

a)
b)
δ^{18}O (‰)
δD (‰)
15
14
13
12
11
10
-70
-75
-80
-85
-90
-95
-100
-105
-110
-115
0
100
200
300
400
500
600
700
800
900
Distance (m)
Monte Almirante
Cuerno Principale below
Cuerno Principale above
Fortaleza
Protolith

Figure 8

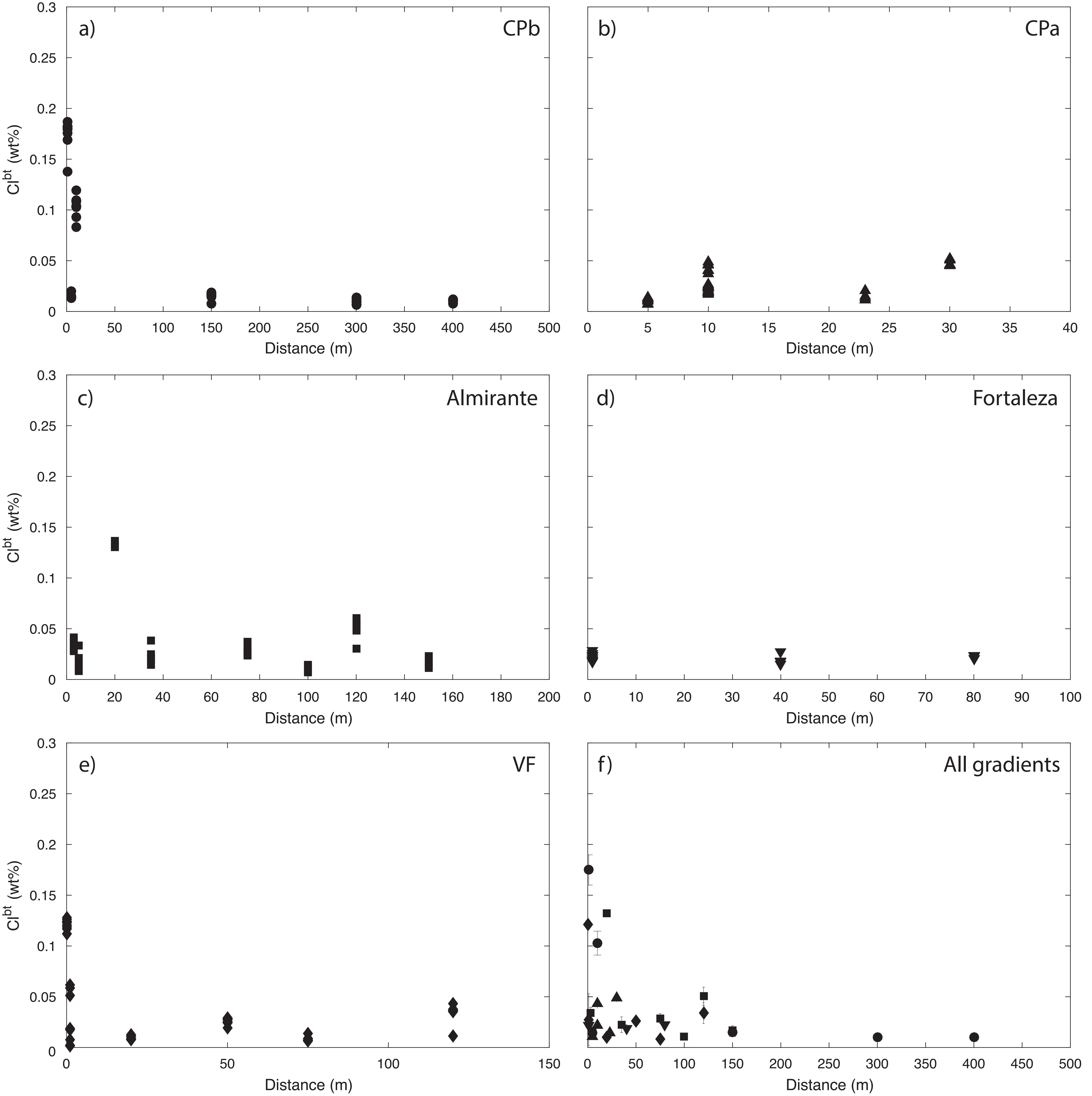

a)
CPb
b)
CPa
c)
Almirante
d)
Fortaleza
e)
VF
f)
All gradients
Cl^{bt} (wt%)
0
0.05
0.1
0.15
0.2
0.25
0.3
Distance (m)
0
50
100
150
200
250
300
350
400
450
500
5
10
15
20
25
30
35
40
20
40
60
80
100
120
140
160
180
200
10
20
30
40
50
60
70
80
90
100
50
100
150

Figure 9

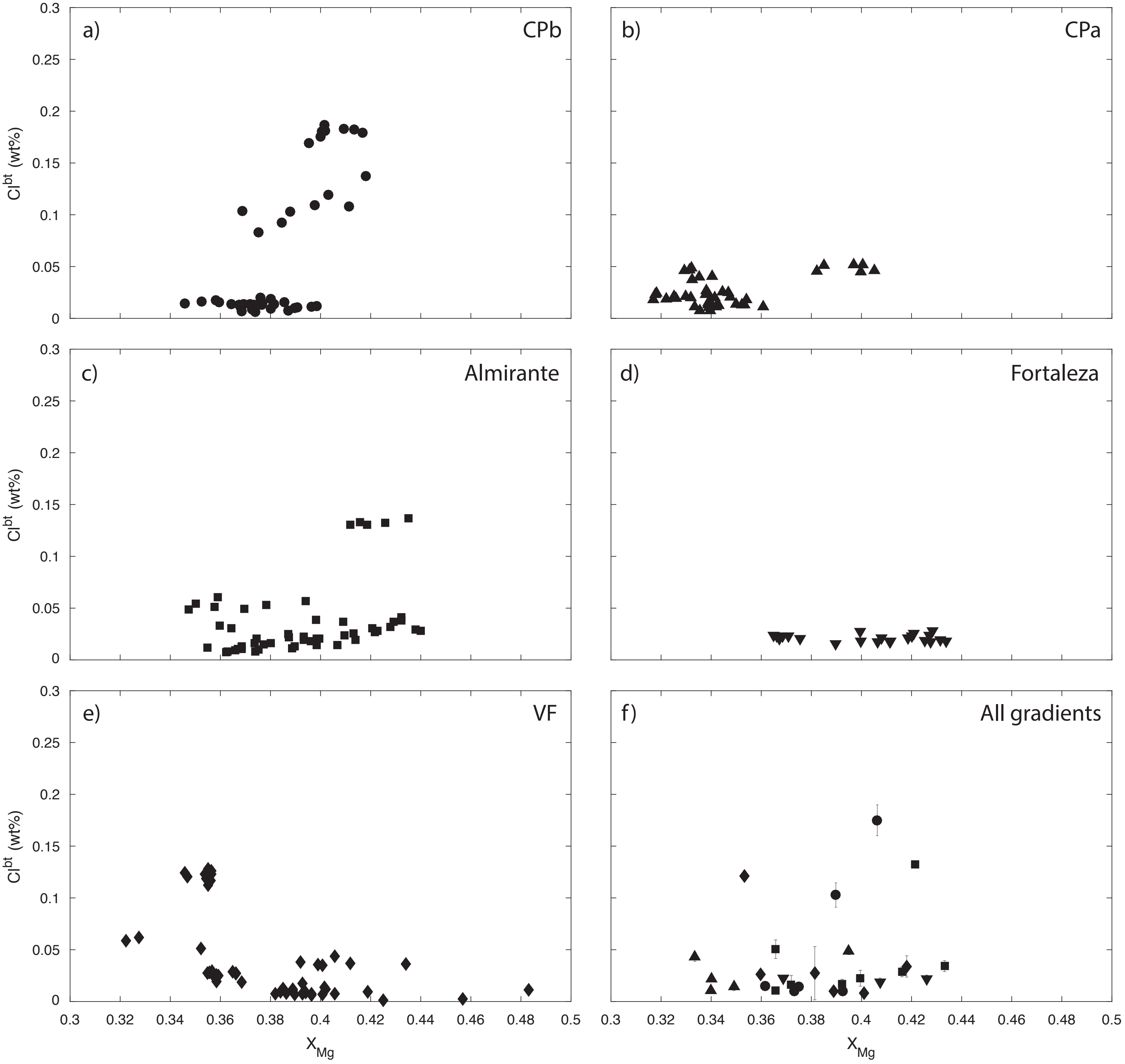
a)
CPb
b)
CPa
c)
Almirante
d)
Fortaleza
e)
VF
f)
All gradients
Cl^{bt} (wt%)
0
0.05
0.1
0.15
0.2
0.25
0.3
0.3
0.32
0.34
0.36
0.38
0.4
0.42
0.44
0.46
0.48
0.5
X_{Mg}

Figure 10

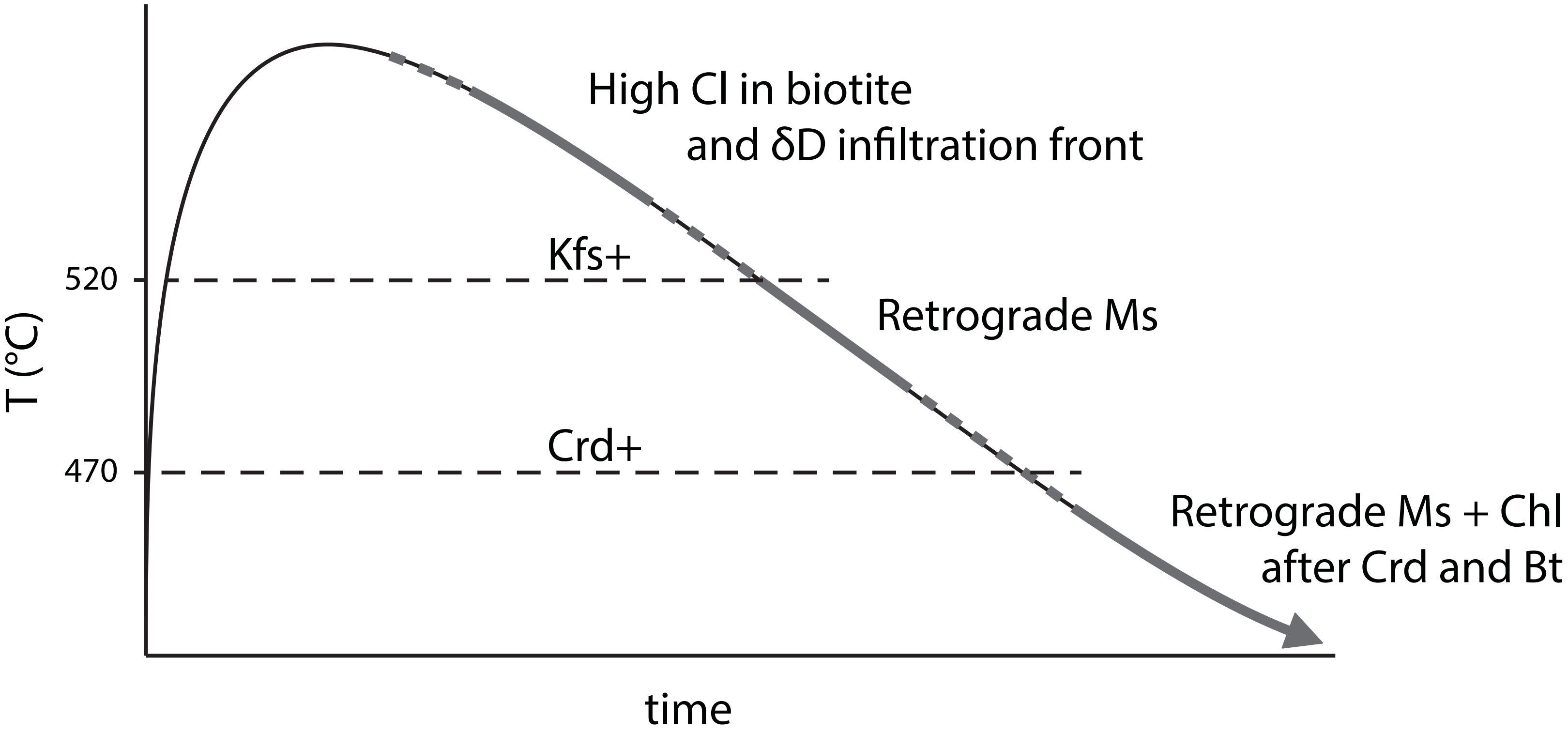
High Cl in biotite
and δD infiltration front
Kfs+
520
Retrograde Ms
T (°C)
Crd+
470
Retrograde Ms + Chl
after Crd and Bt
time